P-13-45

Äspö Task Force on modelling of groundwater flow and transport of solutes

Task 7 – Assessing the significance of flow data in Model Structure Identification

Franz M Krumenacker, The Relief Laboratory

Vesa Keto, VTT Technical Research Centre of Finland

Lasse Koskinen, Posiva Oy

March 2017

Svensk Kärnbränslehantering AB
Swedish Nuclear Fuel
and Waste Management Co

Box 250, SE-101 24 Stockholm
Phone +46 8 459 84 00

ISSN 1651-4416
SKB P-13-45
ID 1419886
March 2017

Äspö Task Force on modelling of groundwater flow and transport of solutes

Task 7 – Assessing the significance of flow data in Model Structure Identification

Franz M Krumenacker, The Relief Laboratory

Vesa Keto, VTT Technical Research Centre of Finland

Lasse Koskinen, Posiva Oy

Background

The SKB Task Force on Modelling of Groundwater Flow and Transport of Solutes is an international forum for organisations from several countries involved in nuclear waste disposal and supporting projects at and related to the Äspö Hard Rock Laboratory (HRL). The activity of the Task Force started in the early 1990's and it has been divided into so called Tasks. There has been eight Tasks defined throughout the last twenty years. The Task Force considers conceptual and numerical modelling of groundwater flow and solute transport in fractured rock. Besides proposing, reviewing, evaluating and contributing to modelling work relevant to the Äspö HRL, the Task Force may promote and endeavour similar activity at the participating organisations.

An example of this was Task 7, in which the participating organisation Posiva Oy (Finland) offered a unique dataset collected of a series of hydrotests covering various scales from the Olkiluoto site for further analyses. The Olkiluoto site houses two nuclear power plants with a third one being built, an operational repository of low- and intermediate level radioactive waste, and is selected for the construction of the high level wastes as well. The site has been subject to intensive research for over thirty years.

Each organisation supporting the Äspö HRL is invited to form or appoint a *Modelling Team* that performs modelling of experiments selected by and/or suggested to the Task Force. The modelling efforts of such teams outside the Äspö HRL are supported by their respective "mother organisations". Each team may choose whether to participate in the different modelling tasks. The Task Force meets regularly; during Task 7 there were normally two meetings each year. Task 7 started in the spring 2005 and the final modeling team presentations were given during January 2012 followed by an evaluation of the task in June 2013.

The work of the modelling groups is coordinated using task descriptions developed by the Task Force Secretariat. The input data are provided in numbered, documented deliverables prepared by the Technical Comittee. The descriptions define the objective and scope of models to be developed within the task, together with the data to be used and the required outputs. This report presents work elaborated on the basis of the task descriptions developed within Task 7, and is one of the individual reports written by the Modelling Groups. The reports have a suggested structure to make their comparison feasible. Upon the reports from the Modelling Groups an evaluation report is provided by the Task Reviewer.

Task 7 was structured into three subprojects called Task 7A, 7B and 7C. Because of an unforeseen change in the composition of our Modelling Group, Task 7A was performed by Vesa Keto (VTT) while Task 7B and 7C were carried out by Franz M Krumenacker (The Relief Laboratory).

Objectives and scope

The primary goal of this Task was to investigate the feasibility of reducing the uncertainty of the calculated model responses by incorporating observed flow data besides the head observations. The data set offered for the modelling groups included information on three different scales. Task 7A addressed a long-term (90 days) pumping test inducing a larger effect on the site-scale, Task 7B involved five shorter hydrotests on the block-scale and Task 7C considered the flow system on the near-field (or canister scale).

These experiments and tests were to be studied and understood, then possibly reproduced with numerical models, which also served performance assessment (PA) purposes. The model responses were to be assessed both in terms of head and flow. An important focus was on the role and behaviour of the long, open boreholes present in the flow system. In the light of the site characterisation the retention properties of the geologic environment had to be estimated.

Since similar data sets are or would be available from the Olkiluoto site, it was also a goal to improve the methodology for formal model calibration, DFN modelling, flow and pathline calculations and creating in-fracture microstructure on various scales.

Summary

On the basis of the input data disclosed in the deliverables and their clarifications provided at Task Force Meetings and Workshops, several numerical models were constructed. The numerical solutions in all the three subtasks were performed using the finite element method as implemented in the FEFTRA modelling package for groundwater flow, transport and heat transfer developed at VTT.

Task 7A

The 90-day-long pumping test around the KR24 borehole in the place of a future ventillation shaft was modelled using the Equivalent Porous Medium (EPM) approach. The interpretation of the geometry of the large, deterministic hydrogeological zones of the site as of 2006 was used in two different settings called 'extended' and 'small' depending on the lateral extension of the hydrogeological zones. This geometry was further developed as part of the calibration, e.g. by introducing a fictitious subhorizontal zone (called 3H) connecting KR24 and the upper part of KR04. The geometry was discretised and converted into an EPM model with the FEFTRA/octree adaptive, automatic mesh generator based on the algorithm of similar name. Both steady-state and transient simulations were performed. The calculated drawdown results were further corrected assuming radial flow around the borehole to overcome the inherent inaccuracies of the linear finite elements.

The calibration of the model was based on the Ensemble Kalman Filter, which is a Monte Carlo approximation of the original Kalman filter. The processing of the stochastic results was performed with the functions implemented in the R statistical package. The calibration produced clearly sharper uncertainty bounds (i.e. narrow probability distribution); and in the majority of the hydrogeological zones the gain proved significant from including the PFL data besides the head observations.

Work performed in the Task 7A1 project was documented earlier by Keto and Koskinen (2009).

Task 7B

A block-scale DFN model was developed to reproduce the interference tests performed in the boreholes KR14 – KR18. The FEFTRA package was complemented with a DFN modelling tool (VINTAGE module). The objective of the modelling was to determine the validity of various alternative DFN definitions with respect to the observed heads and flow distributions. Hundreds of stochastic numerical models (created mostly in either 10 or 20 realisations for each) were generated and assessed. Both steady-state and time-dependent problems were addressed. All parameters in the definition of the stochastic DFN geometry were varied (orientation and size distribution, fracture intensities). The lognormal distribution defined for the transmissivities correlated with the size of the fractures, the level of correlation was also varied. The stochastic DFN was complemented with the site-scale, deterministic hydrogeological zones that fell into the modelled volume. On the basis of the observed responses two more horizontal sheet joints were added to the deterministic hydrogeological zones in a subset of models. The transmissivities of these sheet joints were determined in a formal model calibration procedure based on the Ensemble Kalman Filter.

Because of the relatively low gradient, the role of the DFN geometry and transmissivities became significant in the results. The variability of the calculated flows was large and showed a strong dependence on the actual realisation of the stochastic inputs and on the values of the DFN definition. Several input combinations resulted in invalid models, in which the connectedness fell below the percolation level. Model realisations, which eventually produced qualitatively meaningful results appeared to overestimate the observed flows. The main result of this subtask was the achieved development in the methodology of DFN modelling and in the application of the Ensemble Kalman Filter for a DFN model.

Work performed in the Task 7B project is documented in Chapter 1.

Task 7C

Flow was characterised in the near-field scale, based on observations of head and flow distributions in a field experiment, which had been performed at the locations of three planned shafts of the ONKALO facility. Numerical models were developed around boreholes drilled prior to the excavation of three shafts in their place. On the basis of the observations, the mean transmissivites of a single deterministic fracture and of some stochastic background fracturing were determined using three submodels around the three shafts.

Subsequently, the phase of the bored shafts was considered, which provided exceptionally large hydraulic gradients under which the shaft inflow distribution was measured along the intersection circle of the deterministic fracture and the shaft. This dataset served as a basis for identifying the microstructure of the fracture, with transmissivities assumed to follow a spatially correlated Gaussian distribution conditioned on the observations at the boreholes. The transmissivity field was generated by a matrix factorisation algorithm, using overlapping regions over the modelled area to increase computational efficiency. Experiments were performed with several input combinations to assess the various inputs' role in the model responses. Results included the head fields, the flow distribution, pathlines and the retention properties of the media. It was shown that the results were affected by several factors like correlation length, mean and spread of the transmissivities, or assymetric boundary conditions but also non-physical factors like the arithmetic precision and the discretisation scheme employed in the numerical model.

Based on the experiences gained in Task 7C on the in-fracture heterogeneities a spatially correlated Gaussian transmissivity field was applied in the TS28 simulation case defined in Task 7B to assess the relevance of this field under different circumstances (block scale, smaller hydraulic gradient).

Work performed in the Task 7C project is documented in Chapter 2.

Main conclusions

The three subtasks addressed issues specific to groundwater flow and transport problems on different scales at the Olkiluoto site, Finland.

Task 7A was perhaps the most successful attempt when it comes to reducing uncertainty. The implementation of the Ensemble Kalman Filter and the demonstration of its capabilities were convincing enough that this method has since been used in other projects as well.

Task 7B was a step up too in methodology development. The FEFTRA modelling package was complemented with a DFN tool called VINTAGE, of which applicability was demonstrated on the block scale. The Ensemble Kalman Filter was used in a simpler pilot project involving DFN models. It was recognised in this project that the calculated results can be rather sensitive to the definition of the DFN, especially when the hydraulic gradient is relatively low and because of the scale of the model the flow affects still a considerable volume of rock. Besides the geometry of the DFN, also the distribution of its hydrogeological properties were recognised as a significant factor especially for the flow field. In the assessment of the models' performance and also in the calculation of the flow field the absence of model conditioning in terms of both geometry and transmissivities proved adverse in the DFN models, which marked the direction of the necessary further developments. The recognition of the variability of some of the results across DFN realisations was certainly a new finding in this project. Calibration of a DFN model proved rather hard.

Task 7C required the use and the acknowledgement of the role of microstructure both for a single fracture and in a mixed settings (Task 7C1 and TS28). Task 7C2 appeared unique in that it produced probably the best numerical results with the least effort, which might be attributed to the correct conceptual models and the – probably fortunate – choice of the modelling approach, which actually involved model conditioning. It is open to question if uncertainty was reduced in this task, but some of its sources were identified nevertheless.

A common experience to all the three tasks was that in the course of the modelling process the re-interpretation and to some extent also some additions to the data were necessary for acceptable results. In Task 7A and 7B the given structural model was challenged by complementing it with local features, and in Task 7C the boundary conditions called for adjustments to better represent the model's connection to the outside world. Note that all the three adjustments were based upon available data even if the mainstream conceptual models did not support them.

Lessons learned and implications for Task 7 objectives

The three different scales required very different tools to interpret the input, build the numerical representation of the modelled phenomena and to postprocess the predictions. This, e.g. made it challenging to create models on a unified scale, like the re-calculation of the TS28 simulation case in Task 7B using the microstructure developed in Task 7C.

The use of PFL measurements to reduce uncertainty in models

It was demonstrated in several approaches and modelling experiments that the inclusion of PFL data in the modelling process either improved the results or reduced their associated uncertainty.

In Task 7A the PFL observations were employed in several ways: (a) establishing connectivity between the pumped KR24 borehole and the observation holes, (b) refining the transmissivity distribution over the HZ20A zone, (c) developing assumptions about the channelisation of the flow system and (d) creating *a priori* distributions for the Ensemble Kalman Filter during calibration. The latter conspicuously demonstrated that the reduction of the variance of the predictions (which can be interpreted as a measure of prediction uncertainty) is further decreased if PFL observations are added to the input.

In the block-scale Task 7B a less sophisticated, albeit instructive sensitivity study was used for model calibration, which was based on an *ad hoc* scoring system. The PFL (as well as head) measurements were used for developing scores for 130 sensitivity cases to assess them during the calibration. The scores included information from the comparison of the observed and the predicted frequencies of the flow magnitudes. It was demonstrated that the sensitivity case selected on the basis of both head and flow produced responses closer to the observations than as if either only head or only flow would have been considered.

Task 7C made extensive use of flow data as well, either to obtain transmissivity values at the observation holes (7C2), which were honoured later in model conditioning, or to characterise the microstructure of a fracture (7C3, but in this case the flow distribution was obtained in the nappy experiment, not from PFL readings).

Influence of open boreholes

Earlier experiences and studies (Konikow and Hornberger 2006) showed as well that long, non-pumping, open boreholes influence the flow system, and this study supported similar observations. Without open drillholes the effect of the undisturbed groundwater table of the island remained limited to shallow a depth, but when the open drillholes were present, the groundwater table influenced even the deepest parts of the bedrock. In the presence of pumping this effect appeared in that the long, open boreholes restricted the growth of the hydraulic gradient and homogenized the head field.

Notwithstanding the decreased hydraulic gradient, the shortcut effect of the open boreholes connects areas possibly subject to different pressures, which causes the alteration of the geochemical composition of their environment. The mixing of waters which would not otherwise get in contact with each other may render the vicinity of the borehole non-representative chemically. In more serious cases contaminants may travel along the hydraulic gradient in the borehole, leading to various environmental problems at their destination. This effect is more pronounced with long screens or without appropriate casing, which is in fact specific to many boreholes drilled in crystalline rock.

Open drillholes also provide new flowroutes for groundwater, which was demonstrated especially in the Task 7A simulations with shorter zones not extending as far as the boundaries of the model.

Note that the inclusion of long open boreholes in a numerical model was not straightforward because of the very high contrast of their properties with regard to the rock matrix. Especially challenging was the case of the non-pumped observation holes with no sink or source boundary condition directly attached to them. To avoid numerical problems in the course of solving the model certain measures had to be applied, including pronounced mesh refinement around the borehole, exercising special care to minimise the contrasts, adjusting the parameters affecting convergence in the numerical model, and possibly the postprocessing of the obtained results.

Contents

1 Assessing the significance of flow data in Model Structure Identification: Task 7B

1.1 Abstract

The FEFTRA groundwater flow and transport modelling package was complemented with a DFN modelling tool (VINTAGE module). A block-scale DFN model was developed to reproduce the interference tests performed in the KR14–KR18 boreholes at Olkiluoto, Finland. The objective of the modelling was to determine the validity of various alternative DFN definitions with respect to the observed heads and flow distributions. Hundreds of stochastic numerical models (created mostly in either 10 or 20 realisations for each) were generated and assessed. Both steady-state and time-dependent problems were addressed. All parameters in the definition of the stochastic DFN geometry were varied (orientation and size distribution, fracture intensities). The lognormal distribution defined for the transmissivities correlated with the size of the fractures, the level of correlation was also varied. The stochastic DFN was complemented with the site-scale, deterministic hydrogeological zones that fell into the modelled volume. Beyond this sensitivity study, on the basis of the observed responses two more horizontal sheet joints were added to the deterministic hydrogeological zones in a subset of models in order to explore the validity of an alternative conceptual model. The transmissivities of these sheet joints were determined in a formal model calibration procedure based on the Ensemble Kalman Filter.

Because of the relatively low gradient the role of the DFN geometry and transmissivities became significant in the results. Most probably because of the absence of conditioning the DFN model on the actual borehole data the variability of the calculated flows was large and showed a strong dependence on the actual realisation of the stochastic inputs and on the values of the DFN definition. Several input combinations resulted in invalid models, in which the connectedness fell below the percolation level. Model realisations, which eventually produced qualitatively meaningful results appeared to overestimate the observed flows. The main result of this subtask was the achieved development in the methodology of DFN modelling and in the application of the Ensemble Kalman Filter.

1.2 Sammanfattning

Ett DFN-modelleringsverktyg (modulen VINTAGE) har lagts till grundvattenflödes- och transport-modelleringspaketet FEFTRA. En DFN-modell i blockskala har utvecklats för att modellera de interferenstest som utförts i borrhålen KR14-KR18 på Olkiluoto i Finland. Målet med modelleringen var att bestämma inverkan av olika alternativa DFN-modeller med avseende på de observerade tryck- och flödesfördelningarna. Hundratals stokastiska numeriska modeller (ofta skapades antingen 10 eller 20 realisationer för varje) genererades och bedömdes. Både stationära och tidsberoende problem modellerades. Alla parametrar som ingår i definitionen av den stokastiska DFN-geometrin varierades (orienterings- och storleksfördelning, sprickintensiteter). I den lognormala fördelningen som definierar hur transmissivitet korrelerar med sprickstorlek, var även graden av korrelation varierad. Den stokastiska DFN-modellen kompletterades med de deterministiska hydrogeologiska zonerna som sammanföll med den modellerade volymen i platsskala. Utöver denna känslighetsstudie, inkluderades ytterligare två horisontella zoner (bankningsplan), baserat på de hydrauliska observationerna, till de deterministiska hydrogeologiska zonerna. Detta gjordes i en delmängd av modellerna för att undersöka eventuella förbättringar av denna alternativa konceptuella modell. Transmissiviteterna för bankningsplanen bestämdes i en specificerad modellkalibreringsprocedur baserad på Ensemble Kalman Filter.

På grund av den relativt låga gradienten blev påverkan av DFN-geometrin och transmissiviteterna signifikanta för resultaten. Förmodligen på grund av avsaknaden av konditionering av DFN-modellen på uppmätta borrhålsdata, var variabiliteten hos de beräknade flödena stor och visade ett starkt beroende av de stokastiska parametrarna som definierar DFN-modellen i de olika realisationerna. Flera parameterkombinationer resulterade i ogiltiga modeller, dvs där den hydrauliska genomsläppligheten sjönk under perkolationsnivån. Modellrealisationer, som till sist producerade kvalitativt meningsfulla resultat verkade överskatta de observerade flödena. Huvudresultatet av denna deluppgift var den uppnådda utvecklingen i metoden för DFN-modellering och tillämpningen av Ensemble Kalman Filter.

1.3 Yhteenveto

Työssä FEFTRA virtaus-ja kulkeutumismallinnusohjelmistoa täydennettiin rakoverkkomallinnukseen (DFN) soveltuvalla modulilla (VINTAGE). Olkiluodon kairanrei'issä KR14–KR18 suoritettujen vuorovaikutuskokeiden toistamiseksi kehitettiin lohkomittakaavan DFN-malleja. Mallinnuksen tavoitteena oli selvittää erilaisten vaihtoehtoisten mallien kelpoisuus suhteessa havaittuihin hydraulisiin korkeuksiin ja virtausjakaumiin. Selvitystä varten luotiin ja arvioitiin satoja tilastollisia numeerisia malleja, joista useimmat koostuivat 10 tai 20 realisaatiosta. Tarkasteluja suoritettiin sekä tasapainotilanteessa että ajasta riippuvana. Lisäksi varioitiin sekä DFN-geometriaan liittyviä parametreja (suunta- ja kokojakauma, rakointensiteetti) että lognormaalisti jakautuneen rakotransmissiviteetin ja rakojen kokojakauman korrelaatiota. Tilastollisia malleja täydennettiin sekä tutkimusalueen mittakaavan deterministisillä hydrogeologisilla ruhjevyöhykkeillä että havaittujen vasteiden perusteella kahdella vaakasuoralla raolla, joiden transmissiviteetit määritettiin Ensemble Kalman Filter menetelmään perustuvalla kalibroinnilla.

Suhteellisen pienen hydraulisen gradientin takia DFN-geometrialla ja -transmissiviteetillä oli merkittävä vaikutus tuloksiin. Todennäköisesti DFN-mallin ehdollistamattomuudesta johtuen laskettujen virtaamien hajonta oli suuri ja ne olivat erittäin riippuvaisia DFN-realisaatioiden ominaisuuksista. Useat parametrikombinaatiot johtivat käyttökelvottomiin malleihin, joissa rakojen konnektiviteetti oli perkolaatiotason alapuolella. Toisaalta ne realisaatiot, jotka lopulta johtivat kvalitatiivisesti järkeviin tuloksiin, yliarvioivat havaittuja virtaamia. Tämän osatehtävän pääasiallisena tuloksena olivat edistysaskeleet, jotka saavutettiin DFN-mallinnusmenetelmässä ja Ensemble Kalman Filter kalibroinnin soveltamisessa.

1.4 Introduction and objectives

1.4.1 Scope and objectives of Task 7B

The aim and scope of Task 7B is to simulate the performance of the groundwater system and its response to different interference tests in the presence of open and sealed-off boreholes, by building and assessing the sensitivity of numerical groundwater flow models in the region that accomodates the KR14–18 boreholes at the Olkiluoto site. An important aspect of the data from the site is the use of the Posiva Flow Log to measure flow into/out of the boreholes during "undisturbed" and pumped conditions and the possibility to compare this kind of "flow response" data to "pressure response" data in the same boreholes. Task 7B is divided into three main parts, 7B1 through 7B3.

Task 7B1 is a conceptual task, addressing model boundary conditions, the characterisation of the background fracture population, a plan to iteratively improve the models, compartmentalisation analysis and extracting flow distributions from the models in order to compare them to the observations.

Task 7B2 is a series of modelling exercises based on the concepts, including the conceptual model(s) developed in Task 7B1. These exercises consist of forward and inverse modelling of steady-state and transient head as well as flow distributions. Finally, on the basis of these experiences performance assessment (PA) flow distributions are determined at pre-defined PA boundary conditions.

Task 7B3 addresses questions related to the lessons learned in Task 7B, the role and significance of the input parameters, the background fractures, evidence on compartmentalisation and the reduction of uncertainty.

1.5 Task specifications

1.5.1 Task 7B – Block scale

The Task 7B specification was defined by Vidstrand et al. (2015). The conceptual models were built for the KR14–K18 simulations using the data listed in Table 1-1. The primary differences between these models were the boundary conditions, which were based on data listed in Table 1-2. All the five models were subsequently used in the simulations (Table 1-3) defined in the Task Specification.

Table 1-1. Data incorporated in the conceptual models.

Data	File
Data of single-borehole PFL tests of KR14–KR18 and KR15B–KR18B as fracture specific transmissivity values with fracture orientation and geological parameters.	OL-KR14–18 All Fractures.zip (includes nine files: KR##_Fractures.xls)
Transmissive fractures found by PFL but corresponding fracture in core not identified	Fractures without geoparameters.xls
Geometry of the HZ-model 2008	HZ-08_faces_rev_20080312.txt, HZ-08_20080409.dwg, HZ-08_20080409local.dwf
Ground surface topography	Topography.txt

Table 1-2. Relevant data for the boundary conditions used in the simulations of the KR14–KR18 tests.

Data	File
PFL measurements of KR15–18, KR15B–KR18B, while pumping in KR14 (including data without pumping)	FDOL15A14AF1-final.xls etc.
PFL measurements of KR14,16–18, KR15B–KR18B, while pumping in KR18 (including data without pumping)	FDOL15A18AF1-final.xls etc
Packed-off measurement at KR15–18, KR15B–KR18B, while pumping in KR14 and KR18	OLKR15 pressure observations.xls etc
Packed-off measurements of KR14–17, KR15B–KR18B, while overpressures by HTU in KR17 and KR18	OLKR15 pressure observations.xls etc
Packer locations in KR14–KR18 and KR15B–KR18B	Packer intervals of KR14–18.xls
Pumping rates and drawdowns during PFL measurements	summary of head and pumping.xls

Table 1-3. List of simulations.

Name	Description	Boreholes	Purpose
SS20a	Natural conditions	No boreholes	Forward
SS21	Natural conditions	Boreholes are open and free to cross-flow	Calibration
SS22	Natural conditions	Boreholes are packed-off	Calibration
SS20b	Natural conditions	No	boreholes Based on calibrated models after SS21 & SS22
PA20c	PA conditions	No boreholes	Forward
SS23a	Pumping in KR14	Boreholes are open and free to cross-flow	Forward
SS23b	Pumping in KR14	Boreholes are open and free to cross-flow	Calibration
SS24a	Pumping in KR14	Boreholes are packed-off	Forward
SS24b	Pumping in KR14	Boreholes are packed-off	Calibration
SS25a	Pumping in KR18	Boreholes are open and free to cross-flow	Forward
SS25b	Pumping in KR18	Boreholes are open and free to cross-flow	Calibration
SS26a	Pumping in KR18	Boreholes are packed-off	Forward
SS26b	Pumping in KR18	Boreholes are packed-off	Calibration
TS27	Pumping in KR15	Boreholes are open and free to cross-flow	Forward
TS28	Pumping in KR14	Boreholes are open and free to cross-flow except for one isolated flowing structures in other boreholes	Forward
PA29	PA conditions	No boreholes	Forward

1.6 Task 7B

1.6.1 Modelling approach

Overall approach

The problem formulation in the beginning of Task 7B was whether the block scale representation of the site could be approximated with a parsimonious statistical description of background fracturing. In the solution the PFL measurements were to be used, if possible, and to address the problem the necessary tools had to be developed. The numerical solution was based on the finite element and the finite element analysis was to be carried out with the existing FEFTRA groundwater flow and transport modelling package (Löfman and Mészáros 2013). Besides forward modelling the applicability of inverse modelling tools were to be tested, of which one of the attractive approaches was the Ensemble Kalman Filter, earlier employed in Task 7A. The study had to include extensive sensitivity analysis.

Data usage and interpretation

The data sets defined in the task description were extensively utilized. HTU data was disregarded as no HTU modelling was performed. Initial fracture intensities were based on the HydroDFN database, later these values were updated with data directly available from the boreholes. The transmissivity and the size distributions were derived from the available data as well, along with the boundary conditions and the PFL dataset used in the calibration.

Additionally, the given site-scale structural model was complemented with two smaller sheet joints on the basis of *observed head data*. The existence of these structures cannot actually be excluded on the basis of the *available fracture data*, either.

1.6.2 Conceptual model – Task 7B1

It is hereby emphasised that the results were obtained and assessed from different numerical models, for which the underlying conceptual models were developed iteratively. This report only documents the main results and its associated inputs, however, several attempts were performed for the identification of all relevant parameters. Summary of the conceptual model as suggested by Vidstrand et al. (2015) are collected in Table 1-4.

Main assumptions and simplifications

The summary of the relevant assumptions for building the models are the following:

- The DFN model was built from the deterministic hydrogeological zones and from the stochastic background fracturing.
- The hydrogeological zones were interpreted for the site-scale, albeit a block-scale re-interpretation of the measured data was found feasible by adding two sheet joints.
- The transmissivity distribution over the hydrogeological zones was obtained from interpolating the measured values at the borehole intersection, even though several alternative transmissivity distributions would have been possible.
- The transmissivity inside the stochastic fractures was assumed constant, and it correlated to a certain degree with the size of the fracture. The degree of the correlation was explored at nine grades.

The block-scale geological environment of the hydraulic tests was modelled with a Discrete Fracture Network (DFN), which assumes that due to the hydraulic gradient induced by the pumping tests the water only flows along the interconnected two-dimensional fractures while remaining stagnant in the rock matrix. The two major components the DFN model consisted of the large hydrogeological zones of identified geometry called the structural model of the site (Vidstrand et al. 2015) and the stochastic background fracturing of the rock.

The geometry of the large, deterministic hydrogeological zones has been developed for several years over a series of iterative, refined interpretations using geological, geophysical, hydrogeological and geochemical data. The shape of a hydrogeological zone is typically that of a slightly bent geological fault and is defined as a bounded surface assembled from a few dozens of triangles. The structural

models of the Olkiluoto site customarily assume no holes or other type of discontinuity within a certain hydrogeological zone. The size of such a zone may extend to a couple of km^2 on the site-scale and a few hundred m^2 on the block scale. This modelling study was based upon the structural models released in 2008. Several hydrogeological zones intersect in these models, and all intersections were considered water conductive in the conceptual models. In the presence of appropriate hydraulic gradients, the interconnected hydrogeological zones offer pathways for the flow and the material transport. Special care was exercised to preserve the connectivity matrix defined by the geometry of the hydrogeological zones also in their numerical representation, as well as their connectedness to the boundaries that define the hydraulic gradient for the flow.

Table 1-4. Summary of the conceptual model.

Structure/Feature	Deterministic zones	Background rock
Description	Site scale major fracture zones inluded in the block-scale model wo/ re-interpretation.	EPM model: rock matrix between major structures DFN models: stochastic small scale fractures modelled as circular disks of variable orientation and size.
Location and spatial distribution.	As specified in Posiva bedrock model 2008.	EPM model: Volume enclosing the deterministic zones. DFN model: Between HZ19A and HZ20A. Distributions defining geometry: Spatial: Uniform random (Baecher) Orientation: Fisher Size: Power-law
Hydraulic properties (T or K) and storage.	EPM model: geometric mean T from observations of zones. $S_S = 10^{-6}$ m^{-1} obtained experimentally. DFN model: interpolated T-field from observations.	Uniform within the fracture. Fracture transmissivities are truncated log-normal $\mu(T) = -8.3$, $\sigma(T) = 1.2$ $\lg(T_{min}) = -9$, $\lg(T_{max}) = -5$ connected to their size, strength of connection (S_L) varied.
Heterogeneity/microstructure	Interpolation w/ Ordinary Kriging.	None
Aperture/porosity	0.001 m	0.001 m
Orientation	As specified in Posiva bedrock model 2008.	*Trend: 192* *Pole: 79* *Fisher κ: 3.1*
Length scale	As specified in Posiva bedrock model 2008.	Truncated power-law distribution $P(X > x) = (x/x_{min})^{-b}$ $x_{min} = 19$ m $b = 2.5$ $x_{max} = 50$ m
Likely numerical representation.	Finite element mesh of linear triangular elements.	Finite element mesh of linear triangular elements.
Significant uncertainties in description.	None	Single set of fractures may be a crude approximation.
Prior probability distributions for key parameters	N/A	Orientation: Fisher Size: power-law T: log-normal (see parameter values above)
Approach to choice of model volume and setting model boundary conditions	500 m × 500 m × 500 m block centred on KR15. Side boundaries constant head or upper boundary over HZ19A from larger EPM model (for which the groundwater table was applied on its top surface).	
Treatment of boreholes and features intersecting boreholes (e.g. conditioning)	EPM models: Mesh refinement around the boreholes, the Kriged T-field was conditioned on the transmissivities at the boreholes. DFN models: No refinement around the boreholes, no conditioning of realisations on borehole data.	

Besides the site- and block-scale faults, the rock exhibits fracturing on several smaller scales as well, which adds to the connectedness of the flow system. Measured fracture intensities along the boreholes served as the basis of interpretation for the background fracturing of the rock. Unlike the deterministically considered large faults, the properties of the background fracturing only reflect the measured data in a statistical sense via a few parameters. Stochastic fractures were characterised as sets of circular disks defined by statistical distributions for the location of their centre, the orientation of their plane, radius, and transmissivity.

Note that most of the large, deterministic zones were interpreted as site-scale features, albeit a block-scale re-interpretation of the raw data on the fractures may have been feasible. A set of models actually targeted this approach by introducing two block-scale horizontal sheet joints around the top of the KR14–KR18 boreholes, which participated in the hydraulic tests.

Several experiments were performed by assuming various transmissivity distributions over the hydrogeological zones, including homogeneous and kriged fields of various kinds.

Geometrical description

The external boundaries of the model were derived from, but not identical to a 500 m × 500 m × 500 m cube. The top face of the cube was set at z = 0 m, while its vertical faces were aligned to the axes of Olkiluoto coordinate system (practically north-south and east-west). The KR14–KR18 boreholes were set in the middle of the cube so that they would be at a safe distance from the boundaries. However, eventually the actual modelled volume only comprised the space bounded by the HZ19A and HZ20A hydrogeological zones within the cube, since the effect of these large and water conductive zones proved dominant enough so that in the models the background fracturing above HZ19A and below HZ20A could be safely ignored.

Besides these vertically confining two zones also HZ20B an HZ19C reached the modelled volume. The block-scale re-interpretation of the data gave rise to two more horizontal, local sheet joints of about 15 000 m^2 (called UPPER and LOWER) at the borehole area at depths of z = −20 m and z = −50 m, respectively. However, this extension of the structural model was only considered in a subset of the sensitivity cases.

The initial values of the parameters that defined the stochastic background fracture network were obtained from the HydroDFN database. These values were later refined by analysing the fracture data available from the borehole cores. The Terzaghi-corrected P_{10} intensities were considered as P_{32} fracture intensities.

Several model realisations were generated from the same stochastic input, typically a pool of 20 successful realisations was maintained for subsequent assessments. Experience showed that numerous combinations of the above statistical distributions were unsuccessful in that they failed to meet certain criteria necessary to construct a valid numerical model. E.g. flow calculations assume a hydraulic connection between the boundaries representing the source of the water and the sink, however, in a significant percentage of the realisations the fracture intensities fell short of the necessary level to reach the percolation limit. These realisations were discarded with no further analysis. However, realisations with fracture populations which did not intersect all of the packed-off borehole sections (i.e. the locations of the observations) were accepted for meshing, even though this rendered the assessment of the model inherently more difficult.

Similarly to the deterministic zones, the intersections of the stochastic fractures, as well as those between the stochastic fractures and the hydrogeological zones were conceptually considered fully water conductive. Note that some quality assurance checks on the generated meshes revealed that this concept was not always guaranteed by some of the numerical representations of the DFN.

Each realisation gave rise to somewhat different model responses. In the light of the results the DFN input parameters were revisited and adjusted during the manual model calibration and in the sensitivity cases.

Prior to the DFN approach, scoping calculations were performed with an Equivalent Porous Medium (EPM) model. The purpose of this was twofold: first, to assess and understand the basic properties of the flow on the block-scale and secondly, to provide reasonable boundary conditions for the smaller DFN model (Figure 1-1). The external boundaries of the EPM model were chosen iteratively to determine their safe separation lengths from the boreholes participating in the interference tests. The EPM model was built upon the structural model of 2008 (Vidstrand et al. 2015). The rock matrix extended from z = 0 m down to 1 000 m and 1 500 m in depth and was partitioned into horizontal layers of downward growing thicknesses to model the depth-dependent hydraulic conductivity.

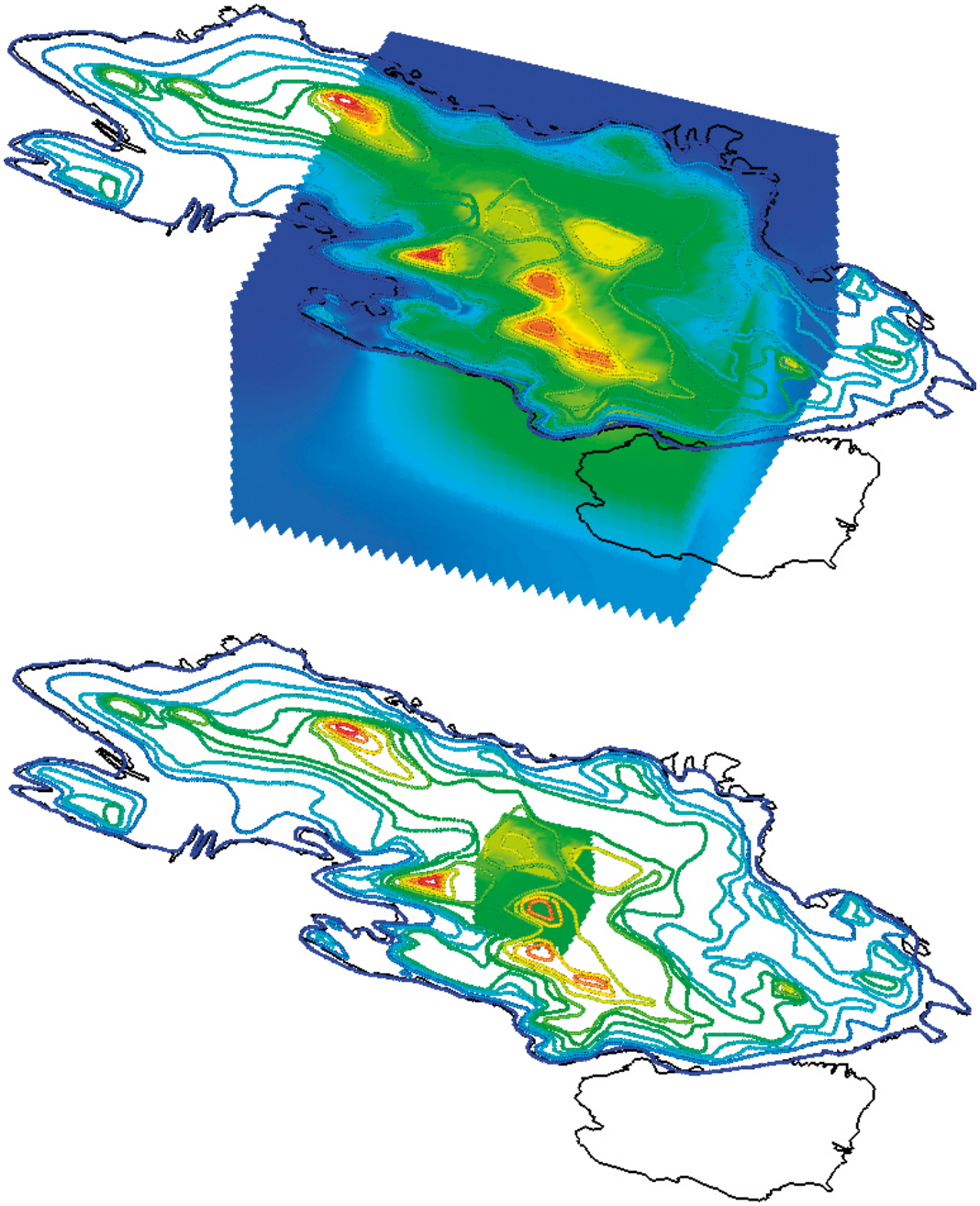

Figure 1-1. *A larger (SS20a) and a smaller (SS23a) EPM model providing boundary conditions for the smaller DFN models.*

Processes considered

The properties and the behaviour of the hydrogeological environment of the borehole area were investigated with a series of steady-state and a few time-dependent (transient) simulations specified in the task description (Vidstrand et al. 2015).

The mathematical models used when determining the steady-state flow along the two- and three-dimensional structures were

$$\nabla(T\nabla h)-Q=0 \quad \text{and} \qquad (\nabla K\nabla h)-Q=0$$

respectively, where

h is the hydraulic head,

T is the transmissivity,

K is the hydraulic conductivity (EPM model only),

Q is the outflow induced by the pumping.

Transient problems were based on the equations

$$\nabla(T\nabla h)-Q=S_t\frac{\partial h}{\partial t} \qquad \text{and} \qquad \nabla(\mathrm{K}\,\nabla h)-Q=S_S\frac{\partial h}{\partial t}$$

where

S_S is the specific storage

S_t is the storativity

The primary result of these simulations was the head field across the modelled volume from which flow distributions along the boreholes were determined using the transmissivities of the fractures.

The head and the flow distributions were affected by the properties of the hydraulic connection between the high-head and the low-head boundaries. This hydraulic connection was determined partly by the geometry of the DFN model, and by the transmissivity distribution along the fractures. Since most of the simulations targeted the solutions to steady-state problems, the relevant parameter in the mathematical model was the transmissivity.

The measured data gave way to several approaches to define the distribution of transmissivity along the deterministic zones. Conceptual models in this study employed an interpolated transmissivity field (with Ordinary Kriging) from the measured data at the borehole intersections (Figure 1-2). The outcome of this type of interpolation is clearly dominated by locally measured values, from which further away the uncertainty associated to the interpolated values grows.

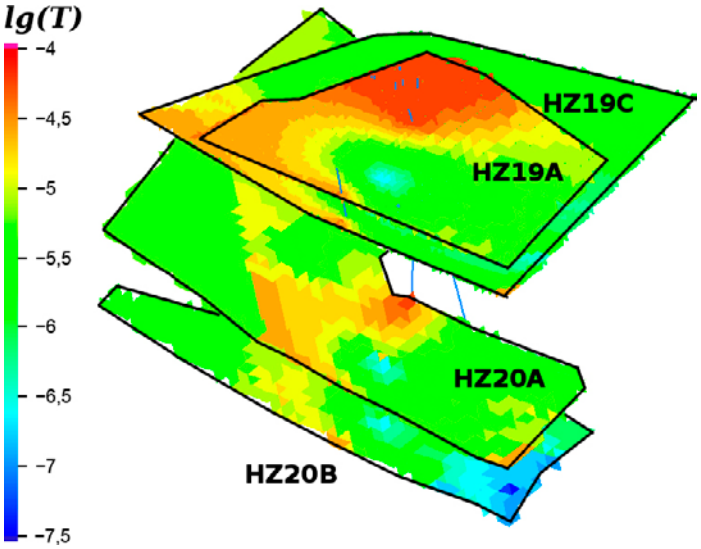

Figure 1-2. *The transmissivity distribution was interpolated for the deterministic zones from the borehole observations by Kriging in the EPM and the DFN models.*

Contrary to the large hydrogeological zones, the transmissivity along each stochastic fracture was considered constant. The actual value of the transmissivity was picked from a truncated log-normal distribution, which could be set to positively correlate with the size of the fracture. The mechanism for this connection between the two different distributions was implemented as follows:

Distribution for fracture sizes follow the power-law probability distribution $f_1(r)$ and fracture transmissivities follow the lognormal probability distribution $f_2(T)$. Let us assume that the corresponding cumulative probability distribution functions for fracture sizes and transmissivities are $y = F_1(r)$ and $y = F_2(T)$, respectively. The cumulative probability function increases monotonically from $y = 0$ to $y = 1$ when r increases from r_{min} to r_{max} or T increases from T_{min} to T_{max}. A random fracture size from the distribution $f_1(r)$ is generated using inverse function of the cumulative probability function $r = F_1^{-1}(y')$ by picking a uniformly distributed random variable y' from a domain [0,1], or $U(0,1)$ for short. A random fracture transmissivity from distribution $f_2(T)$ which is perfectly correlated with the generated fracture size is calculated as $T = F_2^{-1}(y')$, where $F_2^{-1}(y)$ is the inverse function of cumulative probability distribution for fracture transmissivity. This assumes that the same y' value of $U(0,1)$ is used for the fracture transmissivity that has been picked to calculate the fracture size. In the case of semi-correlation the fracture transmissivity is calculated as $T = F_2^{-1}(y'+N(0,S_L^i))$, where $N(\mu,\sigma)$ is a normally distributed random variable with μ mean and σ standard deviation, while S_L^i implements the strength of the correlation for the ith fracture set and is a model input. Here again y' is the same random number picked from the $U(0,1)$ uniform distribution when generating fracture size and $N(0,S_L^i)$ is another random number that is picked from a normal distribution with zero mean and standard deviation of S_L^i. The perfectly correlated case is calculated such that the generated fracture size and transmissivity represent the same percentile from size and transmissivity distributions. The semi-correlated fracture size and transmissivity setup adds a random perturbation to the randomly picked percentile value of the fracture size distribution before the fracture transmissivity is evaluated. The amount of perturbation and strength of the correlation is controlled by standard deviation S_L^i, such that small values of S_L^i lead to stronger correlation between fracture size and transmissivity. However, both fracture size and transmissivity still obey their corresponding probability distributions $f_1(r)$ and $f_2(T)$.

The degree of this correlation was varied via the parameter S_L^i connecting transmissivities of log-normal to fracture sizes of power-law distribution, which ranged $0.0001 \le S_L \le 0.2\,500$ in nine steps to explore its influence on the results (Figure 1-3).

In the case of transient simulations the additional model parameter was the storativity, of which value was subject to experimentation. EPM models produced qualitatively correct results with a fairly large range of specific storage values (10^{-20} m$^{-1} \le S_S \le 10^{-4}$ m^{-1}), but finding a storativity value for the DFN model constituted a problem.

The greatest uncertainty in all the inputs was the definition of the DFN geometry combined with the transmissivity distribution over the fractures.

Boundary and initial conditions

The model exchanges matter and energy with the outside world via the boundary conditions. On the block-scale the nature and the choice of this connection were not straightforward, because no natural boundaries offered justifiable sources of water. Thus this connection to the outside world was experimented in two setups. In the first, the source of water (implemented by constant head boundary conditions) was defined over the HZ19A zone on the top of the model and along the perimeter of what was clipped from the HZ20A zone by the model boundaries. In the second approach the lateral boundaries represented the sources of water (Figure 1-4). In both cases the values of the boundary conditions were obtained from the larger EPM model by interpolating EPM results over the HZ19A and HZ20A zones and the lateral bounding faces of the DFN model. In order to obtain consistent boundary conditions, this approach required that all simulations had to be performed also with the larger EPM model using the appropriate pumping rate for the appropriate borehole.

In the transient problems the initial conditions were defined over the top boundaries. When the pumping started the constant head was released over the HZ19A zone (by switching to no-flow boundary conditions for the rest of the simulation time) to let the depression develop freely.

In the initial phase of the modelling also the pumping was implemented as constant head boundary condition, however all DFN modelling was based on nodal flow as the pumping.

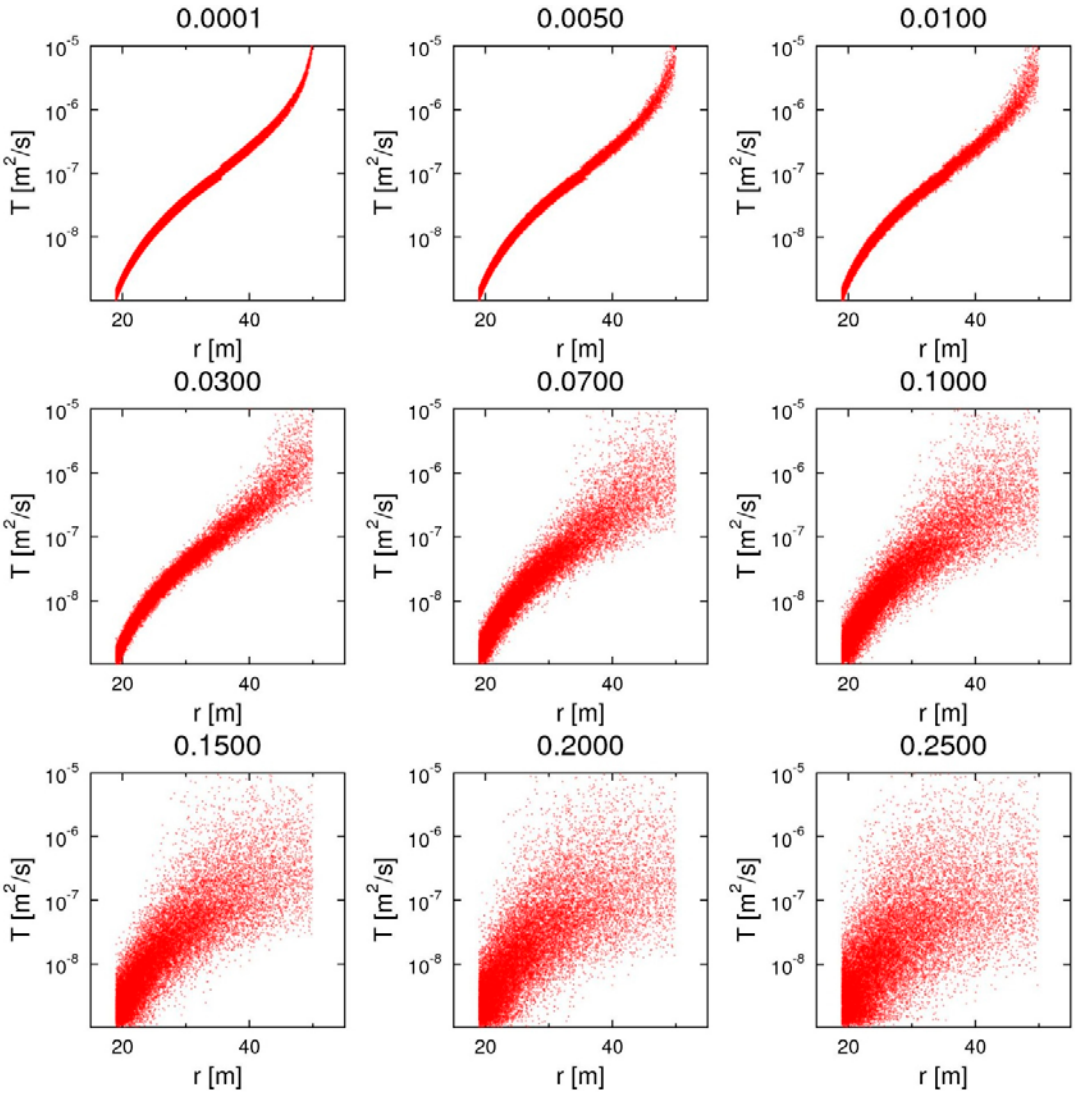

Figure 1-3. *Connection between the transmissivities and the sizes (radius) of the fractures expressed with the S_L parameter $0.0001 \leq S_L \leq 0.2500$. Low S_L values represent strong, high S_L values represent weak connection. In the example shown the log-normal transmissivity distribution was truncated to $-9.0 \leq lg(T) \leq -5.0$ and the power-law size distribution was truncated to $19.0\ m \leq r \leq 50.0\ m$.*

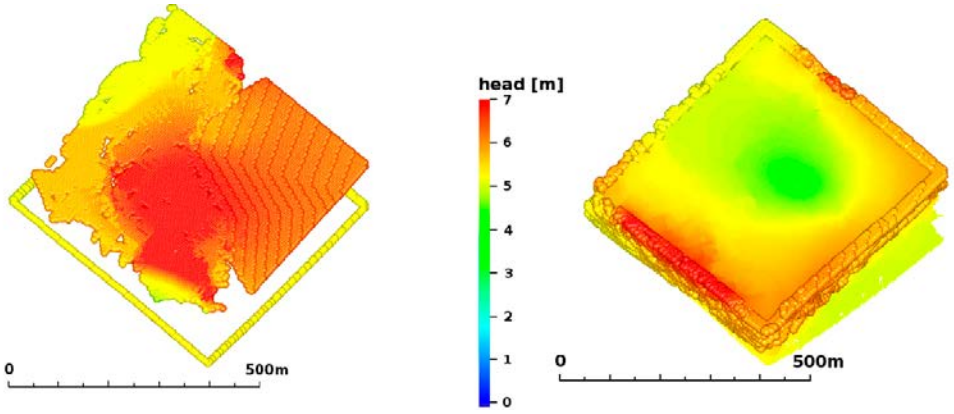

Figure 1-4. *Two approaches were experimented with to define boundary conditions for the DFN model. The SS20a model (left) received head from the undisturbed EPM model on its top and at the perimeter of its bottom. The SS23a model (right) was given boundary conditions on its lateral boundaries so that the drawdown could develop more realistically.*

1.6.3 Model implementation

Numerical model

The conceptual model was implemented in a numerical model and the solution was obtained by finite element analysis. The major challenge was the discretisation of the DFN geometry into a mesh of triangles and their connecting nodes so that the problem could be tackled with the existing finite element tools of the FEFTRA groundwater modelling package.

One of the major objectives in this task was to explore the feasibility and the limitations of a tool for modelling flow and transport in discrete fracture networks (DFN). Similar tools, like FracMan [1] or ConnectFlow [2] have been around for a while, providing insight and experiences on DFN modelling, however, without the control and access to their source code.

The objectives of this work was to develop a tool set that can

- generate a stochastic DFN together with identified, large deterministic fracture zones,
- transform the DFN model into finite elements accessible for a finite element analysis code,
- define boundary conditions for the model,
- solve the model for head,
- compute forward and reverse pathlines using particle tracking as well as
- (the *wl/q* retention properties along the pathlines – used in Task 7C),
- travel times along the pathlines and,
- flow rates across given surfaces and finally,
- extract results from the realisations of the stochastic simulations for visualisation.

Of these tasks the most challenging two were (1) the discretisation of the fracture network into finite elements and (2) the robust implementation of the particle tracking algorithm. It is believed that these problems are common to other DFN implementations as well, thus when using or developing any DFN tool, it is important to understand why these steps constitute difficulties and what are the implications with respect to the results.

There are some, more or less documented approaches to the discretisation problem, like that of FracMan, PAWorks or ConnectFlow – and now the one offered by VINTAGE. Usually, all these tools represent the individual fractures as circular disks, or some sort of approximation of it (like regular n-sided polygons). In the fracture network the individual fractures intersect each other randomly, and these intersections form hydraulic connections between the fractures. In the presence of appropriate boundary conditions these connections give rise to head/pressure differences in the interconnected fracture network. Subsequently, the planes of the fractures along with their intersections provide pathways for particles released from a chosen location in the model. Difficulties arising from the task of discretising this domain in a computationally affordable manner include the resolving of the intersections, approximating low-angle settings, and reproducing the connectivities of the geometry in the numerical model.

FracMan obtains the target set of finite elements that represent this intricate geometry by triangulating the fractures such that the triangles attempt to preserve the geometry of the intersections as well. Experience has shown that this process of triangulation is very complicated and involves a lot of floating-point calculations with all its implications. This may considerably limit the number of realisations which can be assessed in a project.

PAWorks, also a tool developed by the FracMan Technology group, discretises the intersections into a network of pipes, i.e. one–dimensional elements. However, assessing the retention properties of the network obtained this way and especially comparing them to those of a true two–dimensional representation is not always easy or feasible at all.

The available documentation of ConnectFlow suggests that the discretisation of a DFN is performed by a novel algorithm, however, a detailed and comprehensive documentation of this approach is yet to be found. Checking the – otherwise seemingly correct – results calculated by ConnectFlow is thus problematic. In order to address and overcome these issues, another DFN tool based on somewhat different approaches has been developed.

The algorithm

The fundamental idea of this project is that the fracture network, represented by floating–point numbers as their centre points, corner coordinates, etc. is transferred into integer space, where – recognising that integer calculations are a lot faster with a computer – the fractures are recursively subdivided into triangles of unit size by using only fast, integer arithmetic, then the discretised fracture network is transferred back into real–world coordinates. It has been shown that this process is orders of magnitude faster than actually solving the model for the head distribution, thus the discretisation process does not constitute a bottleneck in the modelling.

The particle tracking algorithm, which makes use of the primary results and the pre-generated transmissivity field, is a rather classic, albeit tailored approach to the DFN model.

VINTAGE proper

Even though the notion VINTAGE (Virtual INTeger Arithmetics for Generating Elements) appears as a reference to the toolset responsible for a whole range of tasks from generating the fracture to the calculation of flow rates, etc. in fact the functionality of the VINTAGE proper only covers the discretisation of the fracture geometry into finite elements. The rest of the funcionality (producing the DFN geometry, saving finite element mesh, the associated transmissivities and the prescribed boundary conditions) is considered as auxiliary services.

The DFN geometry and its properties are created from given statistical distributions. The random number generator is based on a Mersenne Twister (Matsumoto and Nishimura 1999). Using FracMan terminology, the spatial model is Baecher (meaning that the centre points of the fractures follow a homogeneous Poisson process in 3D space), and the fracture size is chosen from a power–law distribution:

$P(X > x) = (x/x_{\min})^{-b}$

The transmissivity distribution of the fractures is log-normal and is set to correlate with the fracture size.

Once the DFN geometry has become available consisting of circular disks of known size and orientation, the next step is their discretisation into triangular finite elements. The indicated performance of the discretisation algorithm, however, assumes certain conditions. These are:

The initial shape of the geometry to be discretised must be a regular triangle. As the initial triangle is transferred into integer space, its sides are halved and four new triangles are formed. The new triangles are halved recursively as long as their sides are longer than the unit. This approach creates triangles of good quality (an indispensable requirement for the finite element method) if and only if the initial triangle is regular (Figure 1-5).

It follows that all initial geometry, be it a stochastic fracture or a deterministic fracture zone, must be decomposed first into sets of regular triangles. Fortunately, in the case of stochastic fractures this is not a severe constraint as the conceptual circular disk can be efficiently approximated by regular hexagons, which are in fact composed of six regular triangles (Figure 1-6).

The recursive subdivision of the regular hexagons continues until the appropriate level of detail is reached (Figure 1-7).

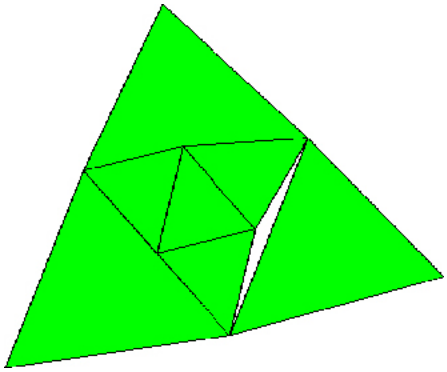

Figure 1-5. *The initial triangle recursively subdivided in the second step of the halving process.*

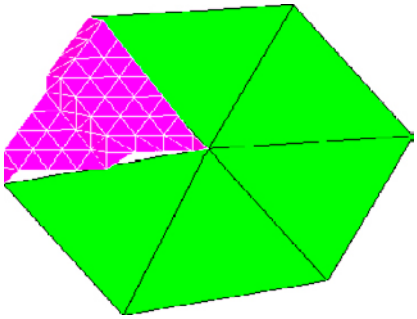

Figure 1-6. *The geometrical representation of a stochastic fractures is a circular disk, which is approximated with a regular hexagon. This can be decomposed into six regular triangles.*

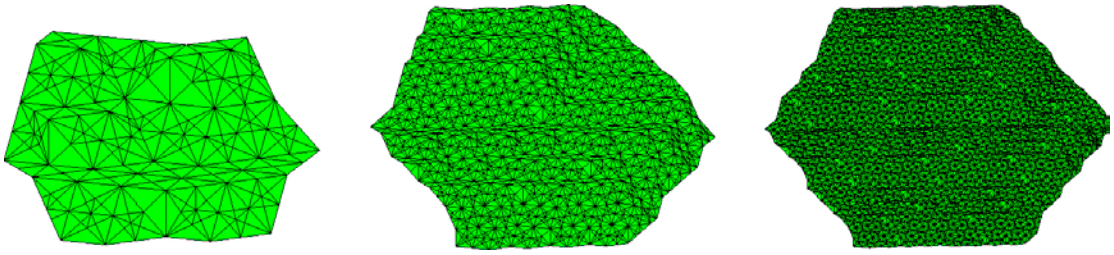

Figure 1-7. *The same fracture was discretised using different recursion levels. The different discretisation levels result in different approximation accuracy, but also affect the size of the problem.*

In the case of large, deterministic fracture zones of irregular shape the decomposition into regular triangles is somewhat more difficult, but is still feasible (Figure 1-8). The algorithm which creates the triangles over arbitrary shapes is based on the topological concept of free edges, which form a closed curve along the perimeter of the complex surface representing a given zone. The implemented process commences with an initial set of triangles as a first approximation for the geometry of the actual zone and terminates when only one loop (the perimeter of the zone) can be assembled from the free edges of the finite elements. This approach is more complex and less efficient than what was described about the discretisation of the hexagons, but usually there are overwhelmingly more stochastic fractures than deterministic zones in the DFN model, thus the presence of the latter does not really affect the performance of the meshing process.

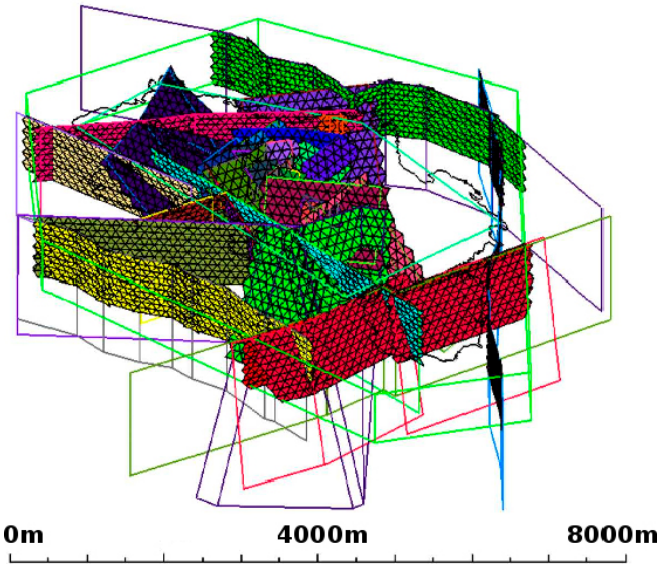

Figure 1-8. *The deterministic zones are discretised into triangles using a different algorithm. Eventually they make part of the finite element mesh specification the same way as the triangles representing the stochastic fractures.*

(Recent developments in the discretisation scheme of VINTAGE improved the connectivity between fractures by dividing the triangles further, however, during the Task 7B project these were not present in the code, hence they are not documented here.) The integer subspace, in which the discretisation takes place, must be of cubic shape and the size (translating into resolution) or edge length of the cube must be of 2^k-1, where $3 \le k \le 21$ units. This arrangement has certain beneficial mathematical properties which can be exploited to save computer memory and CPU time. The integer–coordinate points of this subspace will be called nodes, onto which the final triangles are generated. Once this condition holds and the nodes are numbered from 0 to $(2^k)^3-1 = 2^{3k}-1$ in an appropriate way (Figure 1-9), it can be shown that integer coordinates of the individual nodes can be extracted comfortably from the index number of the node. In case R is the resolution (or size, i.e. the number of units) along an edge of the cubic integer subspace, then node index is formed by merging the three integer coordinates (in base-2 or binary form) into a single binary number:

node = {iz :< R binary digits >}{iy :< R binary digits >}{ix :< R binary digits >}

Using

$xcoord = (2^k-1)$

$ycoord = (2^k-1) \cdot 2^k$

$zcoord = (2^k-1) \cdot 2^k \cdot 2^k$

we obtain the integer coordinates as:

$ix = iand(node, xcoord)$

$iy = iand(node, ycoord)/(xcoord + 1)$

$iz = iand(node, zcoord)/(ycoord + 1)$

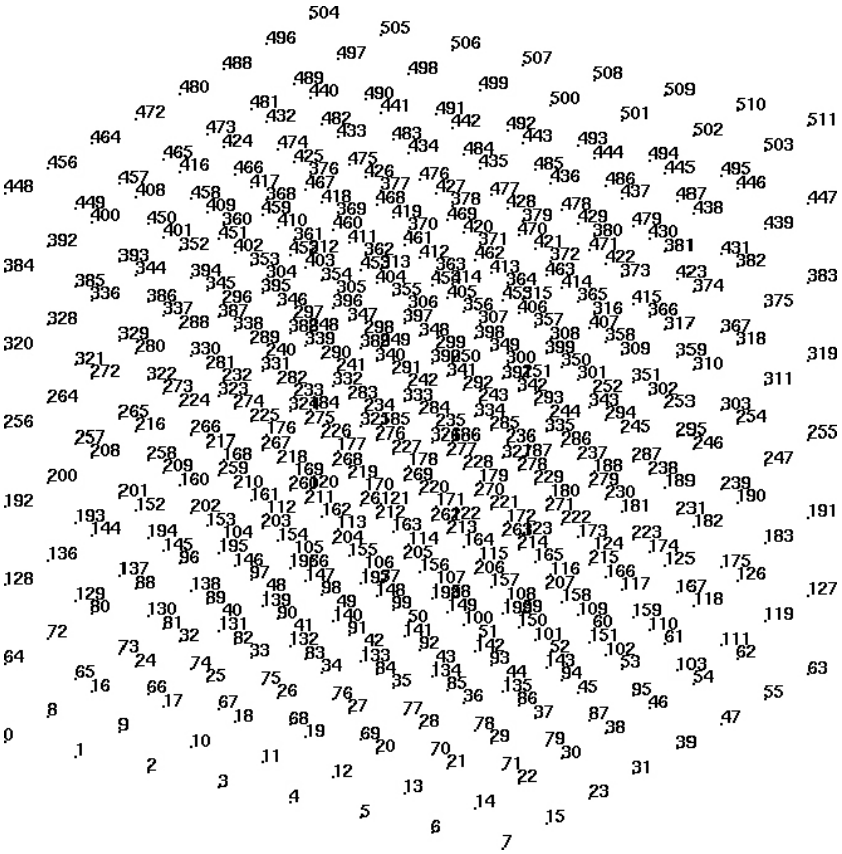

Figure 1-9. *Numbering of the nodes in the integer subspace at k = 3 achieving a resolution of $2^3-1 = 7$. Node indices are assumed to run from 0 to $2^{3k}-1 = 511$.*

where the *iand(iarg1,iarg2)* FORTRAN function performs the binary AND operation on its two integer arguments. Thus the nodal coordinates are never actually stored, only the three nodal indices making up the triangles of the finite element mesh. The resolution is currently limited to $2^{21}-1$ because as of this writing no available FORTRAN compiler supports natively integers greater than $2^{3\cdot21} = 2^{63}$ (INTEGER*8 in FORTRAN terminology). In practice, this is not a bottleneck, as, e.g. the DFNs generated for Olkiluoto were discretised using units of 5−12 m and resolutions of $2^7-1 = 127$ and $2^9-1 = 511$ (i.e. $k = 7$ and $k = 9$, respectively). (In this case the actual bottleneck was the computer memory reserved by the finite element solver.)

The finite element mesh discretising a DFN realisation is illustrated in Figure 1-10**.**

It follows from this algorithm that all the generated triangles are composed of 3 nodes of a unit cube, implying their angles being bounded and the mesh suitable even for transport calculations. It is also true that discretisation on the rectangular grid may limit the sorts of angular relationships occurring in a model. Sub-parallel geometries, e.g. of a monogenetic fracture set caused by a homogeneous stress field would require fine grids.

Further services and potential

Along with its primary functionality, VINTAGE has been designed to perform some other tasks as well, including

- converting the definitions for transmissivity distribution into property lookup tables for the finite element tools,
- calculating the connectivity matrix both in the discrete fracture network and in its finite element representation, with the comparison of the two matrices,
- finding and removing floaters, i.e. the individual fractures or fracture compartments that are not connected to the (case-specific) boundaries,
- setting up boundary conditions by means of auxiliary functions developed for each modelled case, and
- several quality assurance checks, including the visualisation of the inputs over the mesh throughout the code for each phase of the execution.

Of these, tasks involving floating-point calculations on large data sets (like determining the connectivity matrix for a network consisting of 50k+ fractures) are very intensive computationally, sometimes to the extent that they may become prohibitive for multiple realisations. Others, however, especially when the fracture network exhibits considerable connectivity with no floater fractures or multiple-fracture compartments, may become redundant and thus can be switched off altogether.

For the time being an analysis of compartmentalisation is not supported by VINTAGE and thus it was not performed in TaskB, either.

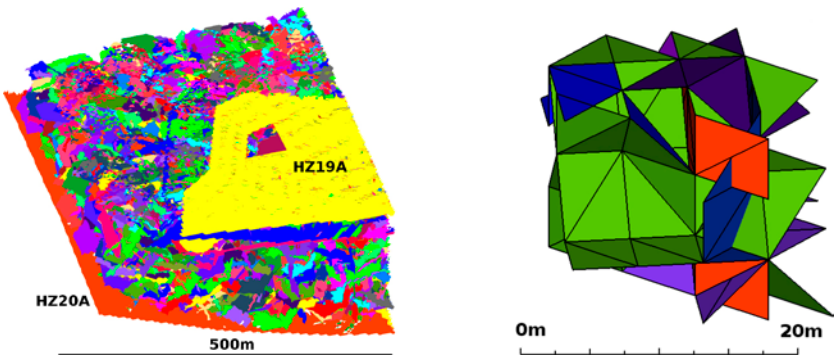

Figure 1-10. *The finite element mesh of the block-scale model (left) and a zoomed-in take of a 15 m × 15 m × 15 m volume (right).*

External boundaries

It is noted here that in the case of a DFN model the concept of an external boundary is different from that of an EPM model. In the latter a topological search may reveal the free faces (i.e. faces only belonging to a single cubic or tetrahedral element) of the finite elements and auxiliary algorithms may subscribe the appropriate boundary conditions on the selected external boundaries. In contrast to this, free faces cannot similarly be identified in a DFN model, which consists only of triangular elements of various orientations in the three-dimensional space. Thus, the external boundaries of a DFN model are taken as a set of nodes falling within a given tolerance from the bounding geometry (e.g. from the relevant face of the modelled cubic volume).

Local coordinates

In the numerical representation of the model the coordinates of the original data were transformed into local coordinates such that from the Finnish UTM coordinates 1 520 000 and 6 790 000 were subtracted, respectively.

Parameters

The input parameters with their range were summarised in Table 1-4, see Figure 1-15 for the result of the SS23b calibration. It is emphasized that a lot of parameters were varied in this study with no intention to find their "right" value, rather, to gain insight in the functioning of the DFN models and their implementation.

Model conditioning and calibration

The objectives of this work did not include a formal calibration of the numerical model, instead, the model's responses to different inputs were assessed in the framework of a thorough sensitivity study. No model conditioning on fracture data was applied, rather, the behaviour of the DFN models was monitored. In the first phase of model evaluation only qualitative assessments and some preliminary manual calibration were performed to gain insight into the weights and effects of the various DFN input parameters. On the basis of these experiences a more orderly approach attempted the evaluation of the model results in the framework of a score system. The scores were calculated from the comparison of the head and flow observations and the model responses. Having ordered the results by a specific score (head or flow) conclusions could be drawn about the relevance of the input DFN data.

Some of the sensitivity cases involved two horizontal sheet joints called UPPER and LOWER, of which transmissivities were estimated by a formal calibration method based on the Ensemble Kalman Filter (EnKF), see Evensen (2009) for a detailed treatment. The main purpose of this exercise was testing the applicability of the EnKF for a DFN model and the validity of the assumption about the two sheet joints.

The EnKF is a recursive filter of which suitability to geophysical and hydrogeological models was explored also in Task 7A. The Monte Carlo approximation of the original Kalman filter is not optimal in the strict mathematical sense but produces useful results of practical significance nonetheless. Unlike in the original Kalman filter, the error covariance matrix is not computed explicitely and propagated in time but it is obtained from the continuously updated ensemble instead. The basic steps of the Ensemble Kalman Filter are the following (see e.g. Chen and Zhang 2006). First, the forecast is performed on each ensemble member independently

$$S_k^{\mathrm{f}}(i) = F\left[S_k^{\mathrm{a}}(i-1)\right] + \mathrm{e}_{1k}(i)$$

where

F is a forecast operator (the flow equation in this case),

S is the state vector, which includes parameters and target variables,

f denotes forecast quantity,

a denotes assimilated quantity,

k is the ensemble member index,

i denotes the time step,

e_1 is the error/noise of the forecast.

(In the initial step the forecast is substituted by a set of a priori generated initial ensemble.)

Then the observation vector at time step *i* for the ensemble members is

$$d_k(i) = HS^t(i) + e_{2k}$$

where
d is the observation vector
S^t is the true value of the state vector
H is the observation operator which represents the relationship between the state vector and the observation vector
e_2 is the error/noise of the observation

The assimilation process starts by calculating the Kalman gain:

$$K(i) = P^f(i)H^T\left[HP^f(i)H^T + R(i)\right]^{-1}$$

where

$$\left\langle S^f(i)\right\rangle \approx \frac{1}{N_e}\sum_{k=1}^{N_e} S_k^f(i),$$

$$P^f(i) \approx \frac{1}{N_e - 1}\sum_{k=1}^{N_e}\left\{\left[S_k^f(i) - \left\langle S^f(i)\right\rangle\right]\left[S_k^f(i) - \left\langle S^f(i)\right\rangle\right]^T\right\},$$

N_e is the number of the ensemble members,
T denotes transpose,
P is the state error covariance matrix,
R is the error covariance matrix of the observations.

Using the calculated the Kalman gain, the updated ensemble of states is:

$$S_k^a(i) = S_k^f(i) + K(i)\left[d_k(i) - HS_k^f(i)\right]$$

and the new (posterior) error covariance matrix is obtained as:

$$P^a(i) = \left[I - K(i)H\right]P^f(i)$$

where *I* is the identity matrix.

In general, the trace of $P^a(i)$ should be less than that of the forecast error covariance $P^f(i)$.

The calibration was performed by a slightly modified version of the EnKF implementation used in Task 7A.

1.6.4 Results – Task 7B2

Outcome of forward and inverse modelling

A typical head field with a realistic drawdown is shown for illustration in Figure 1-11 (SS23b). Note that the vicinity of the pumped area to the model boundary does not constitute a problem as the bottom of the model was defined the conductive HZ20A zone. The lateral boundary conditions represent the source of water. The drawdown remains within a relatively small area. The magnitude of the calculated drawdowns ranged from 2 to 60 m depending on the realisation.

Results of the performed simulations are summarised in Table 1-5, Table 1-6, and Table 1-7.

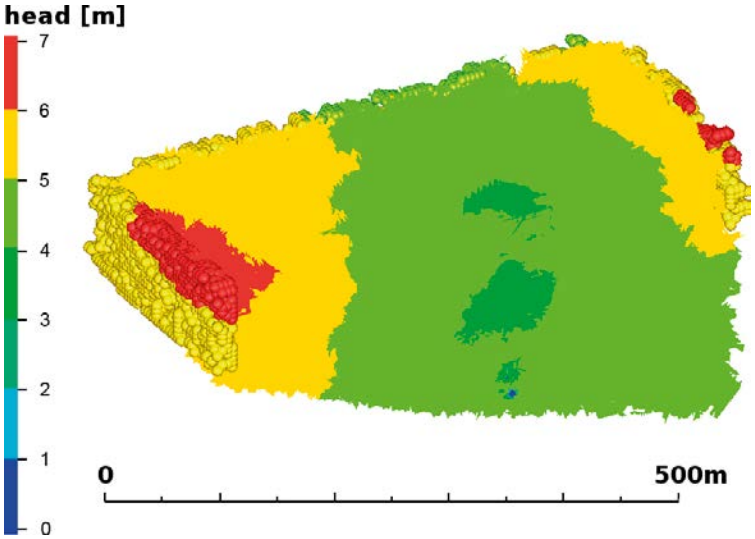

Figure 1-11. *Typical steady-state head field in a vertical east-west cross section.*

Table 1-5. Observed and calculated heads [m] from the steady-state simulation cases with open boreholes.

	SS20a	SS21 observed	SS21 calibrated	SS23 observed	SS23a initial	SS23b calibrated	SS25 observed	SS25a initial	SS25b calibrated
KR14	6.6	7.1	6.6	6.0	5.7	5.8	0.8	0.3	0.4
KR15	6.6	7.0	6.2	3.4	2.9	3.0	3.5	1.5	1.5
KR15B	6.5	7.1	6.7	4.4	1.5	1.2	0.9	0.2	0.3
KR16	6.2	6.9	6.3	3.0	2.4	2.6	3.5	1.4	1.4
KR16B	6.7	7.1	6.7	3.0	2.5	2.5	1.5	0.3	0.5
KR17	6.3	6.9	6.2	3.0	2.4	2.5	3.2	1.5	1.7
KR17B	6.5	8.2	6.7	0.2	2.7	2.4	0.2	0.1	0.2
KR18	6.4	6.9	6.3	3.0	2.7	2.6	10.0	4.0	4.2
KR18B	6.7	7.1	6.8	5.6	2.5	2.3	0.8	0.3	0.3

Table 1-6. Predicted heads [m] from the transient simulation cases with open boreholes.

	TS27 after 1 day	TS27 after 10 days	TS28 after 1 day
KR14	6.7	6.6	−3.7
KR15	5.5	5.3	3.7
KR15B	6.5	6.2	4.7
KR16	6.6	6.6	4.6
KR16B	6.9	6.8	5.4
KR17	6.8	6.7	4.5
KR17B	6.8	6.7	6.5
KR18	6.7	6.6	4.1
KR18B	6.9	6.8	5.6

Table 1-7. Calculated heads [m] from the simulation cases with packed-off boreholes.

Open	SS24 observed 6.8@KR14	SS24a initial 5.1@KR14	SS24b calibrated 3.0@KR14	SS26 observed 8.1@KR18	SS26a initial 5.1@KR18	SS26b calibrated 5.3@KR18
KR14:L1	(open)	(open)	(open)	2.8	1.5	1.6
KR14:L2	(open)	(open)	(open)	0.7	*	*
KR14:L3	(open)	(open)	(open)	0.6	0.2	0.0
KR15:L1	disturbed	*	*	disturbed	*	*
KR15:L2	–	*	*	–	*	*
KR15:L3	1.5	1.1	3.9	0.3	0.2	0.0
KR15:L4	3.4	2.2	4.1	3.5	*	*
KR15:L5	3.5	2.1	4.1	3.6	2.3	2.5
KR15:L6	5.6	1.8	4.1	0.9	1.0	1.1
KR15B:L1	5.7	1.8	4.2	0.9	0.7	0.8
KR15B:L2	4.7	1.7	4.2	0.6	0.3	0.3
KR16:L1	0.5	0.7	5.0	0.3	0.6	0.7
KR16:L2	0.9	0.8	4.9	0.5	0.3	0.4
KR16:L3	2.1	1.5	3.5	2.2	1.4	1.5
KR16:L4	2.4	1.6	3.4	3.9	1.9	*
KR16:L5	3.2	1.8	*	3.7	*	2.5
KR16:L6	3.2	1.7	3.4	3.3	1.0	1.1
KR16B:L1	3.3	1.7	3.3	3.1	*	1.2
KR16B:L2	3.3	1.8	3.4	1.0	*	1.2
KR16B:L3	–	*	*	–	*	*
KR17:L1	0.4	0.1	4.4	–	*	*
KR17:L2	1.3	1.4	5.0	1.2	0.5	0.7
KR17:L3	1.3	1.4	5.1	1.2	0.6	0.7
KR17:L4	3.3	1.6	5.0	3.0	*	1.0
KR17:L5	3.2	1.8	4.9	3.4	2.2	1.4
KR17:L6	3.2	1.3	4.9	3.4	0.9	1.5
KR17B:L1	3.3	1.3	4.7	2.8	0.8	0.9
KR17B:L2	1.7	1.6	4.7	0.5	1.2	1.4
KR18:L1	2.7	1.8	4.9	(open)	(open)	(open)
KR18:L2	2.5	*	4.7	(open)	(open)	(open)
KR18:L3	3.4	*	4.8	(open)	(open)	(open)
KR18:L4	3.4	*	*	(open)	(open)	(open)
KR18:L5	3.2	1.9	4.7	(open)	(open)	(open)
KR18B:L1	6.1	2.0	4.4	0.8	0.3	0.2
KR18B:L2	5.4	*	4.4	0.7	0.0	0.1

* Packed-off borehole sections, which did not intersect any of the fractures in any of the ten realisations could not report a result.

The SS20a results were averaged from 100 realisations, the rest is from 10 realisations. SS23b was actually obtained having analysed 130 cases × 10 realisation/case = 1 300 realisations, but was averaged from the 10 realisation of the "winning" case that scored best in the sensitivity studies. Note that the TS27 and TS28 results are from EPM models.

The evolution of head in the transient simulation cases TS27 and TS28 show a somewhat more pronounced drawdown with respect to the observed 8 m and 10 m at

$S_s = 10^{-6}$ m^{-1} (Figure 1-12).

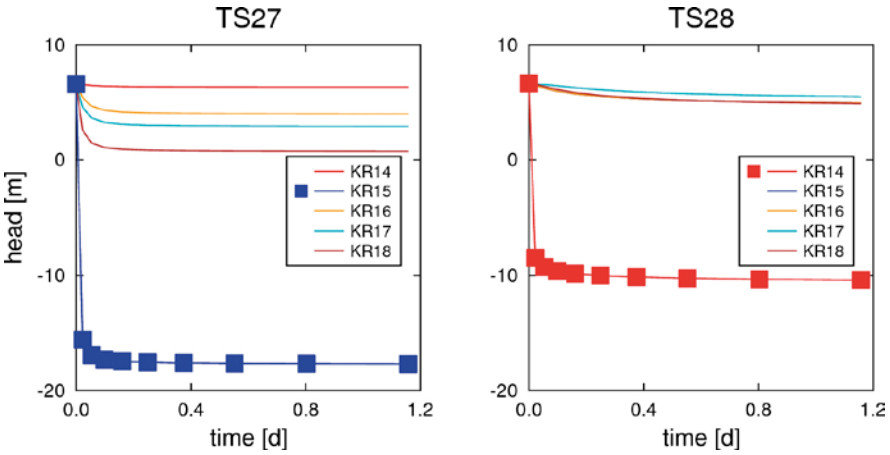

Figure 1-12. *Head histories for the first day of pumping in the TS27 and TS28 simulation cases.*

Model calibration

Calibrating the SS23b simulation case

In this simulation case pumping was performed in KR14, and the boreholes were open and free to flow. During the calibration five parameters of the DFN definition were varied (Table 1-8), resulting altogether 130 cases with 10 realisations each:

Table 1-8. Summary of the calibrated parameters.

Fracture orientation	Fixed parameter	Mean trend 192°	Mean plunge 79°	Dispersion Fisher κ: 3.1
Fracture intensity	Fixed parameter	P_{32} = 0.41 m^2/m^3	Terzaghi-corrected p_{10}	Mean intensity of different boreholes weighted by the used borehole section
Transmissivity distribution	Calibrated parameters	$-7 \le \lg T_{max} \le -5$ $0 \le \sigma(T) \le 1.8$	Truncated log-normal	$\sigma(T)$, $\mu(T)$ $T_{min} \le T \le T_{max}$
	Fixed parameter	$\mu(\lg T) = -8.3$		
	Calibrated parameter	$0.0001 \le S_L \le 0.2500$	Connection between size and transmissivity	
Fracture size distribution	Calibrated parameter	$50\ m \le r_{max} \le 100\ m$	Truncated power-law	
	Fixed parameter	r_{min}, b	Minimum fracture size	Exponent
Presence of sheet joints	Calibrated parameter	Present only in a subset of the cases	*T* was not calibrated here, only their presence	

By varying the above parameters a series of results, in fact several "guesses" were obtained. The decision upon which of these results might best describe the observed values was based on an *ad hoc* score system composed of measures considering flows and heads. On one hand, flow frequencies were calculated from the PFL observations as well as from the 130 calculated cases, averaging over the 10 realisations. As the primary interest was in the flow distribution, rather than in the flow magnitudes, Kolmogorov-Smirnov (KS) statistics (distance and relevance) was used to score the results with respect to the flow distributions (Figure 1-13).

By this measure it became feasible to order the results by the flow KS distance (Figure 1-14 (left)). On the other hand, a further aspect for the assessment of the simulation cases was the root mean square deviation (RMSD) of the observed and calculated heads in the open boreholes, providing another set of scores to order the results (Figure 1-14 (right)). Thirdly, the variability of the flow was also calculated, and was found ranging between $0.63 \le \sigma(Q) \le 1.22$ l/min over the realisations of the 130 sensitivity cases.

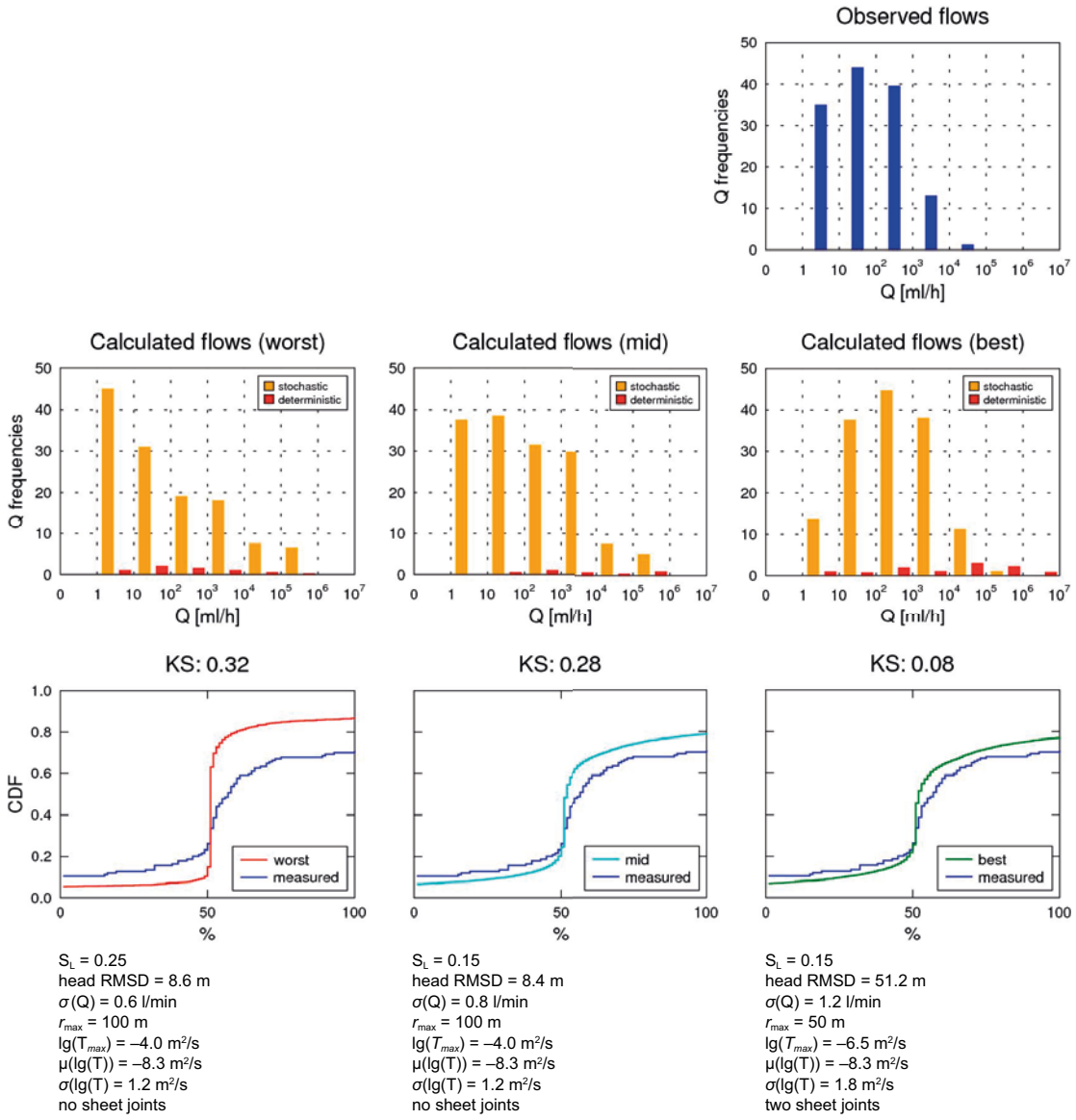

Figure 1-13. *Scoring the calibration cases by their Kolmogorov-Smirnov distances from the observed flow frequencies. Left column: worst scoring sensitivity case, middle column: a sensitivity case that scored on the average and right column: best scoring sensitivity case. Yellow bars: calculated flows from stochastic fractures, red bars: calculated flows from deterministic fractures. Note that the case best scored by Kolmogorov-Smirnov performed very poorly by head Root Mean Square Deviation.*

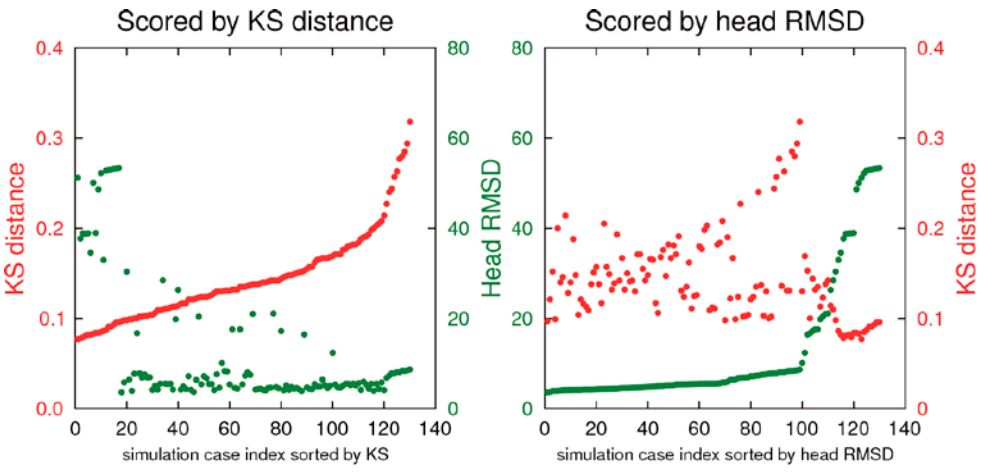

Figure 1-14. *Assessment of the simulation cases by their different scores.*

The score system revealed that a distinct group of the simulation cases fared better than the others in both flow and head (Figure 1-15). The decision about the result of the calibration was based on the minimum of the $\sqrt{RMSD^2 + KS^2}$, but also the variability of the calculated flow was considered. The analysis of these scores has shown that the KS-RMSD-ordered scores exhibit an L-shaped distribution (Figure 1-15), characterized by results of (1) distinctly poor (i.e. high) head RMSD values (this is the top of the „L"), (2) results of distinctly poor (i.e, high) flow KS distances (this is the rightmost part of the bottom of the „L") and (3) by a set which scored relatively well for both measures. Interestingly, no combination of the input parameters scored equally poorly for both the flow KS and the head RMSD measures. Distinctly poor head RMDS scores were obtained in sensitivity cases with low transmissivities (upper truncation $\lg(T_{max}) = -6.5$ m^2/s) and including the two sheet joints. Poor flow KS distances came from cases with larger fractures ($r_{max} = 100$ m) with higher transmissivities (upper truncation $\lg(T_{max}) = -4.0$ m^2/s) and with no strong correlation between fracture size and transmissivity ($S_L \geq 0.07$) .

The SS25b simulation case, in which KR18 was pumped with open boreholes, has not been calibrated in this manner, but simply re-calculated with the above parameters which appeared to perform well in the SS23b case. The simulation cases with packed-off borehole sections were not calibrated either, because with no conditioning of the DFN model on the fracture data at the boreholes, it could not be guaranteed that the DFN and all of the packed-off section would intersect – a precondition to obtaining model responses – at all.

Calibrating the transmissivities of the sheet joints

As an experiment, in a further set of sensitivity case two horizontal, block scale sheet joints (Table 1-9) were added to the deterministic zones at the borehole area (Figure 1-16). The transmissivities of these structures were determined with the Ensemble Kalman Filter as detailed above.

Table 1-9. Corner coordinates of the UPPER and LOWER horizontal sheet joints.

	Local X [m]	Local Y [m]	Z [m]
P^1_{UPPER}	5770	2350	−20
P^2_{UPPER}	5900	2350	−20
P^3_{UPPER}	5900	2480	−20
P^4_{UPPER}	5770	2420	−20
P^1_{LOWER}	5770	2350	−50
P^2_{LOWER}	5900	2350	−50
P^3_{LOWER}	5900	2470	−50
P^4_{LOWER}	5770	2470	−50

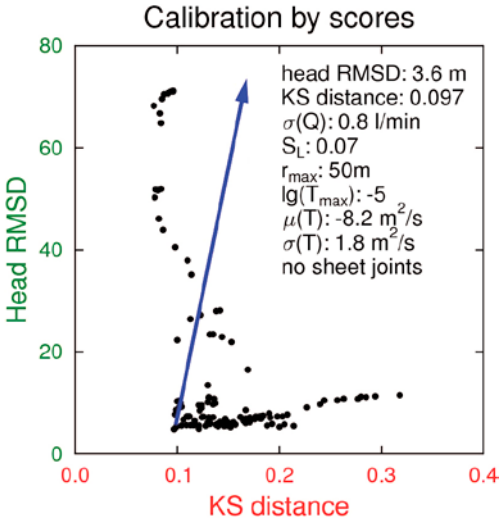

Figure 1-15. *The result of the SS23b calibration was obtained from the unified score.*

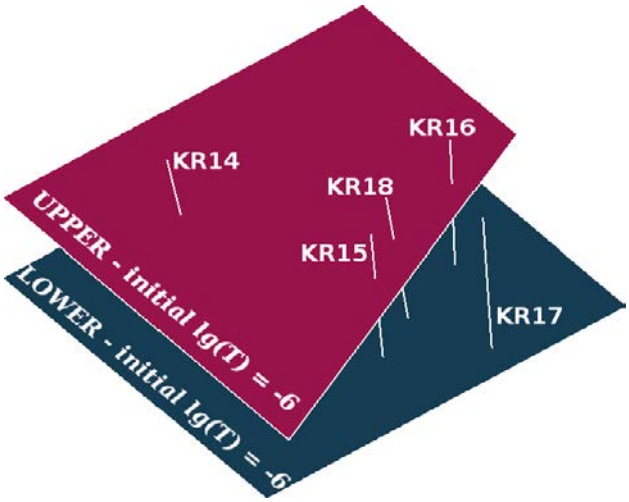

Figure 1-16. *The lay and extension of the added horizontal structures at the borehole area.*

The ensemble size was varied involving between 7 and 14 members. Different initial ensemble populations and *a priori* distributions were tried. Initial mean values for the the transmissivities of the sheet joints were varied by a couple orders of magnitude. The variances of the two model parameters and of the observed heads were set between 10–20% of their mean value. The EnKF algorithm converged (Figure 1-17) invariably and produced similar values in the vast majority of the cases.

In the light of the calibration results the inclusion of the LOWER sheet joint is not necessary, since the transmissivity of the LOWER structure converged to a very low value $\lg(T_{\text{LOWER}}) = -16$. On the other hand, the inclusion of the UPPER structure appears justified with $\lg(T_{\text{UPPER}}) = -4.8$.

Prediction of cumulative flows

Cumulative flows were calculated for several simulation cases and realisations and also as part of the sensitivity studies.

The flow magnitudes (Figure 1-18 and Figure 1-19) varied considerably across realisations of the same simulation case, it is believed that this variability was greater than that among the head fields.

At a fixed DFN geometry the hydraulic connections were varied by changing the correlation between the fracture size and transmissivity (S_L parameter). The re-defined hydraulic connections between the boundary conditions gave rise to distinctly different flow distributions at times almost in a different order of magnitude (Figure 1-20). In the light of these results the models were rather sensitive to the strength of the correlation between the fracture size and transmissivity.

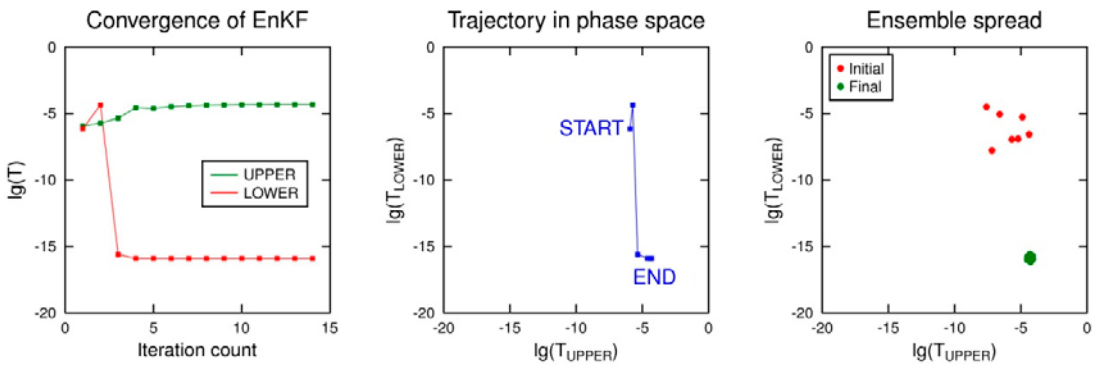

Figure 1-17. *The transmissivities of the two sheet joints converged within a few iteration steps (left). The trajectory of the state vector was calculated as the average of the ensemble members of the actual time step (middle). The calibration successfully reduced the initial variance of the ensemble (right).*

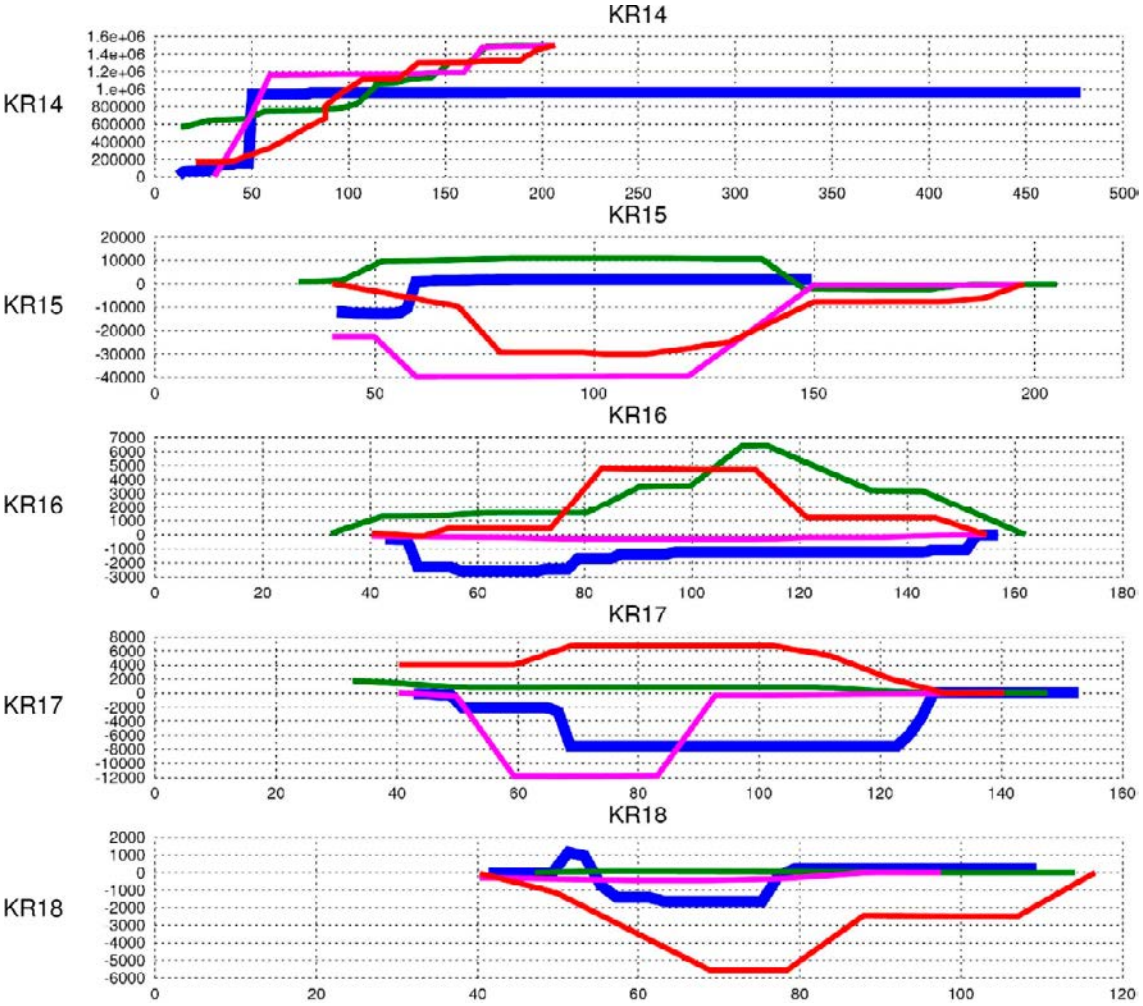

Figure 1-18. *Cumulative flows along the boreholes when KR14 was pumped. Horizontal axis: borehole length [m], vertical axis: cumulative flow [ml/h], positive when water flows out of the borehole. Blue: observed distribution. Green: flows in the realisation considered in best agreement with the observations. Red: flows in the worst realisation. Magenta: flows between the best and the worst.*

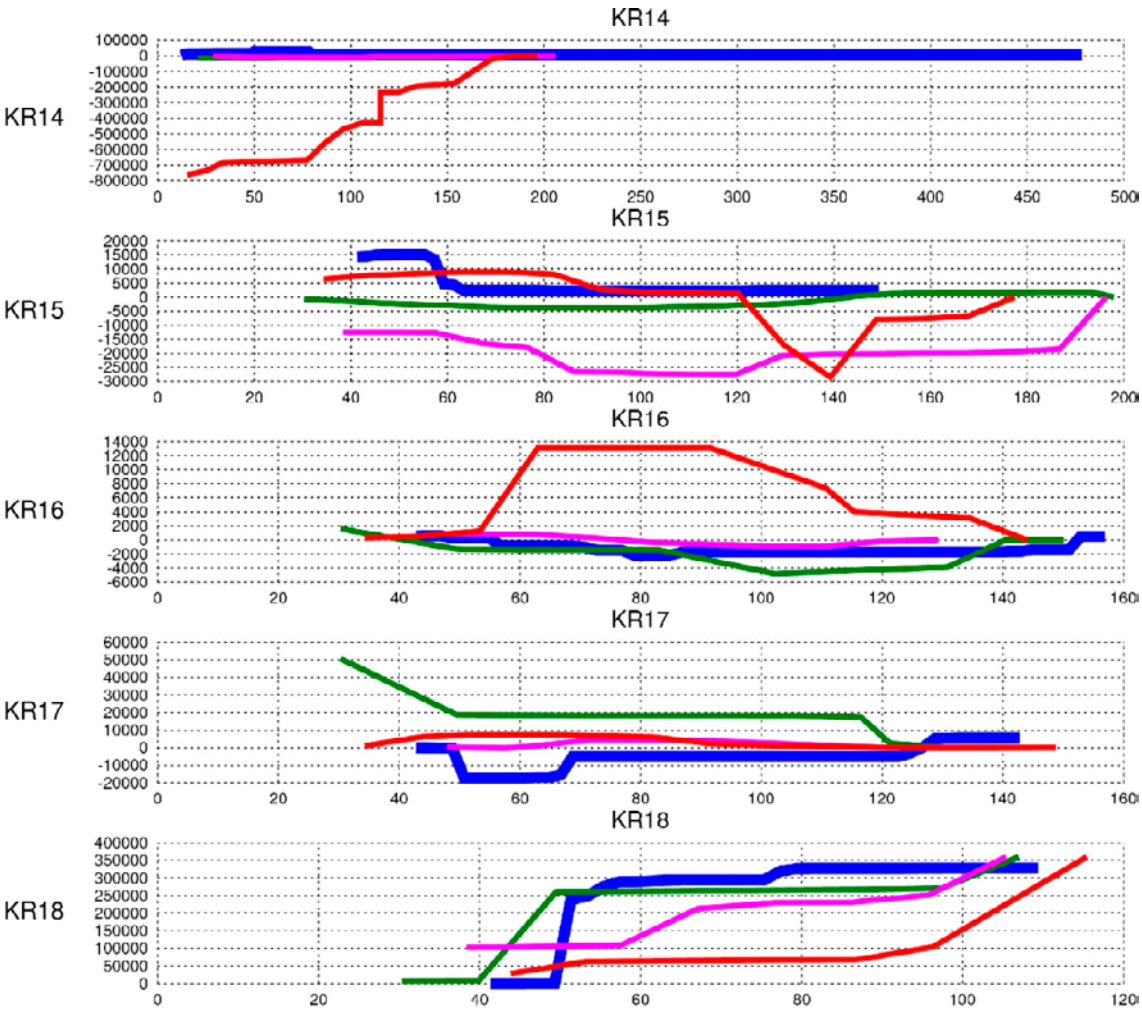

Figure 1-19. *Cumulative flows along the boreholes when KR18 was pumped. Horizontal axis: borehole length [m], vertical axis: cumulative flow [ml/h], positive when water flows out of the borehole. Blue: observed distribution. Green: flows in the realisation considered in best agreement with the observations. Red: flows in the worst realisation. Magenta: flows between the best and the worst.*

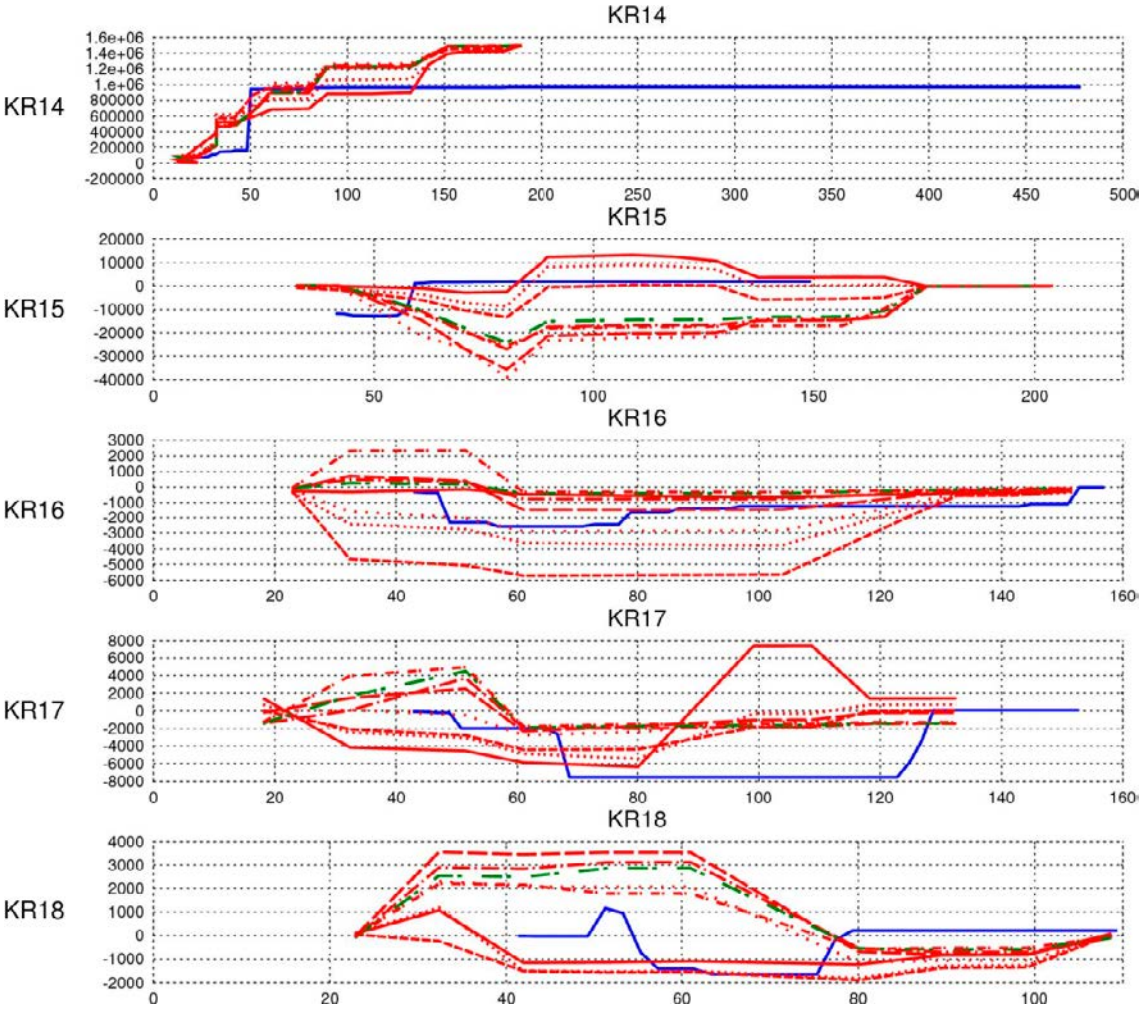

Figure 1-20. *Cumulative flows along the boreholes when KR14 was pumped. Horizontal axis: borehole length [m], vertical axis: cumulative flow [ml/h], positive when water flows out of the borehole. Blue: observed distribution. Green and red dashed lines: calculated at different values of the S_L parameter.*

Extrapolation to PA boundary conditions and particle tracking

Pathlines initiated from the nine locations defined in the performance measures (Table 1-10) are shown for the PA20c and PA29 cases in Figure 1-21, respectively.

Table 1-10. Coordinates of the nine particles released into the Performance Assessment models.

Local X	Local Y	Z
5800	2400	−100
5800	2450	−100
5800	2500	−100
5850	2400	−100
5850	2450	−100
5850	2500	−100
5900	2400	−100
5900	2450	−100
5900	2500	−100

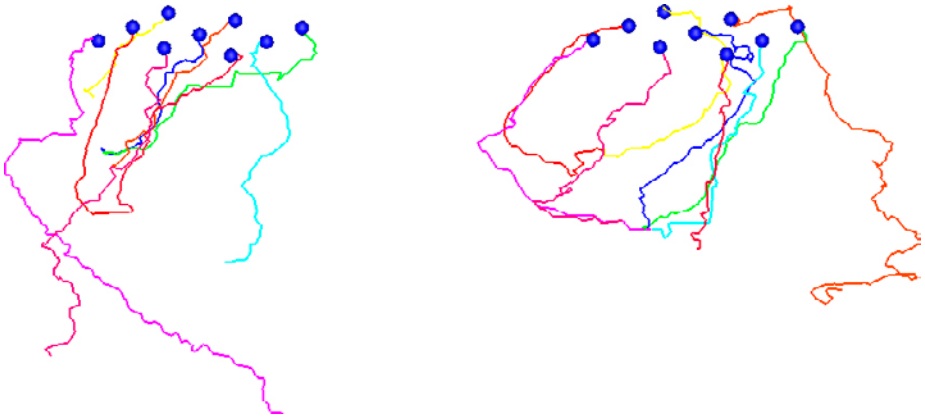

Figure 1-21. *Pathlines in the undisturbed PA cases: PA20c (left) and PA29 (right). The order and the colour coding of the pathlines are identical.*

1.6.5 Discussion and conclusions – Task 7B3

Discussion of results

In assessing the uncertainty associated to the presented results the following points are made.

On the block-scale no natural boundary conditions lend themselves for application, thus the boundary conditions used in this study constitute sources of uncertainty.

The algorithm responsible for the discretisation of the DFN geometry into a finite element mesh may not map the connectivity matrix of the fractures obtained from their geometry into the connectivity matrix determined in the finite element mesh. This may be a consequence of the differing representations of a fracture in the generated DFN and in a mesh. The process of generating a DFN in VINTAGE is currently strongly tied to the shape of a circular disk, because the generation region is populated assuming a certain fracture intensity with fractures of known area, which is obtained from the shape of a circle. The generation of the mesh, however, assumes the shape of a regular hexagon for reasons referred to above.

Basically, two types of error may occur when discretising fractures falling close to each other: (1) the fractures do intersect by their geometrical definition, which is represented as two circular disks, but in the finite element mesh a remaing small gap between the elements representing them leaves them non-connected and (2) the fractures do not intersect in their geometrical representation, yet in the mesh they are erroneously connected by a few nodes (shortcuts). These errors constitute inherent properties of the discretising algorithm and they somewhat affect the development of pathlines and the calculated retention properties. Experience showed that errors of both types occur in a small proportion, of which the erroneous shortcuts are more typical. This means that worse retention properties are calculated from the mesh than from what would follow from the DFN geometry, thus the results err on the side of caution.

The Task 7B project was the first endeavour in which the FEFTRA/vintage module was employed and it also revealed some of its shortcomings, which have been corrected afterwards. Because of these shortcomings, e.g. in the case of flow calculations based on the early version of the code, results should probably be approached with some care.

In assessing the created models and the results, it can be stated fairly certainly that the obtained outputs, however they were based upon the measured values, overestimated the observed flow magnitudes and distributions. A reason for this may be the overconnectedness of the model, which originated either from the geometry of or the transmissivity distribution prevailing in the DFN. As for the geometry, there may be several reasons of a possible inadequacy, e.g. a single set of fractures is insufficient to describe the DFN on the block-scale, or the size distribution (in terms of its parameters and truncation limits) did not fulfill its office, etc.

Experience showed that varying the parameters that define the DFN geometry towards less connectedness only increased the ratio of the realisations falling below the percolation level, but the geometrically valid realisations tended to overestimate the observed flows still.

The connectedness of the model could also be decreased by lowering the truncation limits of the truncated log-normal transmissivity distribution. However, the interpretation of the observations suggested that there are fractures of higher transmissivities present in the background fracturing taking part in the flow system, thus the upper truncation limit of $\lg(T) \leq -5$ was accepted an honoured. Lowering only the lower truncation limit so as to increase the frequencies of less conductive fractures in the model in order that it became less connected resulted only in an increase in the spread of the transmissivity values, which led to numerical instabilities in the course of the finite element analysis.

The problem of model connectedness may suggest that a single set of fractures characterised by a single size and transmissivity distribution may not offer an adequate description of the background fracturing on the block-scale.

Unlike a single-set setup, several fracture sets even with similar DFN properties may form loosely or hardly connected compartments, between which the connection is inferior to what prevails inside them. Since the hydraulic gradient was relatively small in these models, the role of the DFN definition is augmented in the results. A further indication of the inadequate DFN definition may be that the time-dependent simulation cases (TS27 and TS28) could only be calculated with the EPM approach, but no appropriate combination of the boundary conditions and the fracture storativities were found for the DFN models which were able to reproduce the time-dependent EPM results.

The overestimation of the observed flows may also be originated from the inadequately defined boundary conditions. The constant head prescribed at the external boundaries of the steady-state block-scale model constitutes an unlimited source of water flowing towards the sinks, which might be too abundant compared to what is available in the reality in the vicinity of the interference tests. The external boundary conditions might be better modelled as if acting from behind a hydraulic obstacle (skin), similarly perhaps to what the General-Head Boundary (GHB) package implements in MODFLOW. This would render the effective transmissivity of the model less than what would follow from the original definition and consequently, limit the magnitude of the flow.

The variability of the cumulative flows across realisations of the same case was greater than expected. At occasions the most successful realisations remained within the same order of agreement with the observations. This information might be useful in a calibration technique which is able to search for an optimum beyond the statistical description of the DFN (e.g. a genetic algorithm). It has been shown in the sensitivity cases that the correlation level between the fracture size and transmissivity has a marked influence on the results, however the exact nature of this influence is not yet understood. The variability of the flow across correlation levels was higher in the observation holes than in the pumped borehole, which seems intuitively correct. On the other hand, strong correlation between fracture size and transmissivity did not always lead to better flow results – probably because extensive features of high transmissivities often create the potential for shortcuts, which observation borehole flows are rather sensitive to.

The assessment of some of the realisations where no fractures were present at the location of the observations (packed-off borehole sections) failed. It is believed that both of these problems could be tackled by conditioning the DFN on the fracture data along the boreholes.

The calibration of the SS23b simulation case was based on a rather arbitrary score system, and it is open to question if this score system lived up to the expectations at all. Note that the Kolmogorov-Smirnov statistics may reward flow distributions with excess magnitudes in them if the *shape* of the distribution is close to the observed frequencies elsewhere. Thus this approach lends itself to various improvements, e.g. by discarding cases with out-of-range calculated values, etc. In addition, this approach does not guarantee that –in the light of the individual scores –there would be a subset or a member of the population faring distinctly or any better than the rest.

The calibration process using the Ensemble Kalman Filter proved surprisingly efficient and robust. One of the most welcomed properties of this approach was that calibrated results tend to have smaller variance, lending to the interpretation of reducing the uncertainty. Later the parallelisation of this algorithm was implemented, thus this approach may be extended to model calibration tasks involving more variables and more complex cases.

Both the PA20c, PA29 cases and the re-visiting of the TS28 simulation case in Task 7C reinforce what was demonstrated in the calibration of the SS23b simulation case, notably that results are rather sensitive to both the definition of the DFN and the transmissivity distribution. In both cases the boundary conditions remained unchanged and only the underlying DFN model was updated which had a significant influence upon all calculated results: heads, flows and pathlines.

Main conclusions

This study targeted the development of methodology for the creation of stochastic DFN models as well as their quantitative assessment. A DFN modelling tool using fast integer arithmetics and a calibration framework based on the Ensemble Kalman Filter were developed as two new modules of the FEFTRA package. These tools were applied to problems based on field data (observed head and flow) from Olkiluoto and various types of results (calculated head, flow, pathlines and retention properties) were produced with them. Thus one of the main conclusions is that these tools were capable of producing qualitatively correct, credible results. On the basis of this experience these tools would probably perform similarly in other modelling endeavours.

The actual modelling process revealed that (1) it does make a difference how the DFN model is defined, (2) the results show a significant variability depending on the various realisations, and (3) the calibration of DFN models can be difficult. Alternatively to what has been attempted in this study, future work might include conditioning the DFN definitions on the observations available from the cores.

2 Assessing the significance of flow data in model structure identification: Task 7C

2.1 Abstract

Flow was characterised in the near-field scale, based on observations of head and flow distributions in a field experiment, which had been performed in the ONKALO at the Olkiluoto site, Finland. Numerical models were developed around three boreholes drilled prior to the excavation of three shafts in their place. On the basis of the observations, the mean transmissivities of a single deterministic fracture and of some stochastic background fracturing were determined using three submodels around the three shafts.

Subsequently, the phase of the bored shafts was considered, which provided exceptionally large hydraulic gradients under which the shaft inflow distribution was measured along the intersection circle of the subhorizontal deterministic fracture and the shaft. This dataset served as a basis for identifying the microstructure of the fracture, with transmissivities assumed to follow a spatially correlated Gaussian distribution conditioned on the observations at the boreholes. The transmissivity field was generated by a matrix factorisation algorithm, using overlapping regions over the modelled area to increase computational efficiency. Experiments were performed with several input combinations to assess the various inputs' role in the model responses. Results included the head fields, the flow distribution, pathlines and the retention properties of the media. It was shown that the results are affected by several factors like correlation length, mean and spread of the transmissivities, or asymmetric boundary conditions but also non-physical factors like the arithmetic precision and the discretisation scheme employed in the numerical model.

Based on the experiences gained in Task 7C on the in-fracture heterogeneities a spatially correlated Gaussian transmissivity field was applied in the TS28 simulation case defined in Task 7B to assess the relevance of this field under different circumstances (block scale, smaller hydraulic gradient).

2.2 Sammanfattning

Grundvattenflödet karaktäriserades i närområdet av schakt, baserat på observationer av tryck- och flödesfördelningar i ett fältförsök som utfördes i ONKALO på Olkiluoto i Finland. Numeriska modeller utvecklades baserat på data från tre borrhål som borrades på samma ställe där tre schakt senare konstruerades. Baserat på observationerna bestämdes de genomsnittliga transmissiviteterna för en deterministisk spricka och den förekommande stokastiska bakgrundssprickigheten med hjälp av tre delmodeller runt de tre schakten.

Därefter studerades inverkan av de borrade schakten, vilket gav exceptionellt stora hydrauliska gradienter under vilka schaktinflödesfördelningen uppmättes längs skärningscirkeln hos den sub-horisontella deterministiska sprickan och schaktet. Detta dataset tjänade som grund för att identifiera sprickans mikrostruktur, med transmissiviteter antagna att följa en rumsligt korrelerad Gaussfördelning konditionerad på observationerna vid borrhålen. Transmissivitetsfältet genererades av en matrisfaktoriseringsalgoritm och med användning av överlappande regioner för det modellerade området för att öka beräkningseffektiviteten. Numeriska experiment utfördes med flera indatakombinationer för att bedöma de olika parametrarnas roll i modellsvaren. Resultatet inkluderade tryckfältet, flödesfördelningen, partikelspår och retentionsegenskaperna hos mediet. Det visade sig att resultaten påverkas av flera faktorer såsom korrelationslängd, medelvärde och spridning av transmissiviteterna eller asymmetriska randvillkor men också icke-fysiska faktorer som den aritmetiska precisionen och diskretiseringssystemet som används i den numeriska modellen.

Baserat på de kunskaper som uppnåtts i Task 7C angående de interna sprickheterogeniteterna tillämpades ett rumsligt korrelerat gaussiskt transmissionsfält i TS28-simuleringsfallet definierat i Task 7B för att bedöma relevansen av detta fält under olika omständigheter (t ex blockskala samt mindre hydraulisk gradient).

2.3 Yhteenveto

Pohjaveden virtausta kuvattiin lähialueen mittakaavassa perustuen ONKALOsta havaittuihin hydraulisiin korkeuksiin ja virtausjakaumiin. Virtausmallit kehitettiin niiden pilottireikien ympärille, jotka oli porattu kolmen kuilun kohdalle ennen niiden louhimista. Ainoan deterministisen raon ja tilastollisen taustarakoilun transmissiviteetit määritettiin käyttämällä kolmea pienempää mallia erikseen kuiluja vastaavien pilottireikien ympärillä.

Yhdestä kuilusta oli mitattu vuotovedet deterministisän raon ja kuilun leikkauskohdasta poikkeuksellisen suurten louhituista kuiluista johtuvien hydraulisten gradienttien vallitessa. Tämän aineiston perusteella identifioitiin raon mikrorakennetta ja sen transmissiviteetin oletettiin seuraavan spatiaalisesti korreloitunutta Gaussin jakaumaa, joka oli säädetty toteuttamaan havainnot. Laskennallisen tehokkuuden parantamiseksi transmissiviteettikenttä generoitiin algoritmilla, jossa mallinnusalue jaettiin limittäisiin pienempiin osiin. Eri lähtöparametrien vaikutuksia mallin antamiin tuloksiin (hydraulinen korkeus, virtausjakauma, virtaviivat ja kallion pidättymisominaisuudet) arvioitiin kokeilemalla useita eri parametrikombinaatioita. Tuloksiin vaikuttivat useat tekijät kuten korrelaatiopituus, transmissiviteetin keskiarvo ja hajonta, epäsymmetriset reunaehdot, mutta myös epäfysikaaliset tekijät kuten aritmeettinen tarkkuus ja numeerisen mallin diskretointitapa.

Perustuen rakoheterogeenisyydestä osatehtävässä Task 7C saatuihin kokemuksiin spatiaalisesti korreloitunutta Gaussin jakaumaa seuraavaa transmissiviteettikenttää sovellettiin osatehtävässä Task 7B määriteltyyn laskentatapaukseen TS28, jolloin voitiin arvioida kentän kelpoisuutta eri olosuhteissa (lohkomittakaava, pienempi hydraulinen gradientti).

2.4 Introduction and objectives

Objectives and scope of Task 7C

Task 7C targeted the understanding the near-field scale with respect to flow and head responses. The focus of the study was small sub-volumes surrounding three ventilation shafts of ONKALO at Olkiluoto, Finland.

The objectives included the use of the observations obtained with the Posiva Flow Meter (PFL) to characterise, analyse and demonstrate procedures to quantitatively describe low transmissivity ($T \leq 10^{-9}$ m^2/s) fractures.The scope of Task 7C covered four subtasks.

In Task 7C1 the low transmissivity fractures were characterised by borehole, PFL, hydraulic testing and shaft mapping. On the basis of this data the microstructure of the fracture was built.

Task 7C2 was primarily a simulation task for the evaluation of the quantitative microstructural fracture model developed in Task 7C1.

Task 7C3 moved the scale from the near-field to that of a single fracture which intersected the shaft built on the location of the boreholes used in Task 7C1. The target of this study was the reproduction of the observed flow distribution at the fracture-shaft intersection.

In Task 7C4 the uncertainties associated to the necessary assumptions, simplifications and implementation issues found in Task 7C1, C2 and C3 were addressed.

2.5 Task specifications

2.5.1 Task 7C – Single-fracture scale

The task specification suggested a cylinder or a box as the frame of the conceptual model with no-flow on the top and on the bottom boundaries and constant head on the sides.

Data relevant for the construction of the conceptual model (Vidstrand et al. 2015) were provided in the task deliverables as:

Data	File
Fracture trace geometries	Fracs.dwg/Fracs.dxf
Fracture and PFL	Fracture and PFL data of task 7C_v1.zip
Detailed mapping, photos, water leakage values	Nappy-results and traces in KU2.zip

Data relevant to the boundary conditions (Vidstrand et al. 2015):

Data	File
Borehole geometry data	Borehole_paths.zip
Shaft wall geometries (section surrounding fractures)	Fracs.dwg/Fracs.dxf

The following simulations were to be carried out for Task 7C1 and 7C2. In the names of the simulations the ’s-’ stands for single-hole tests and the ’c-’ stands for cross-hole tests as references to the notation used by Posiva.

Name	Description	Boreholes	Purpose
s-PP122	Tool for calibration	Borehole PP122 open and PFL measured Boreholes PP123, PP124, PP126, PP128 closed	Characterisation of fracture
s-PP123	Tool for calibration	Borehole PP123 open and PFL measured Boreholes PP122, PP124, PP126, PP128 closed	Characterisation of fracture
s-PP124	Tool for calibration	Borehole PP124 open and PFL measured Boreholes PP122, PP123, PP126, PP128 closed	Characterisation of fracture
s-PP126	Tool for calibration	Borehole PP126 open and PFL measured Boreholes PP122, PP123, PP124, PP128 closed	Characterisation of fracture
s-PP128	Tool for calibration	Borehole PP128 open and PFL measured Boreholes PP122, PP123, PP124, PP126 closed	Characterisation of fracture
s-PP131	Tool for calibration	Borehole PP131 open and PFL measured Boreholes PP134, PP137 closed	Characterisation of fracture
s-PP134	Tool for calibration	Borehole PP134 open and PFL measured Boreholes PP131, PP137 closed	Characterisation of fracture
s-PP137	Tool for calibration	Borehole PP137 open and PFL measured Boreholes PP131, PP134 closed	Characterisation of fracture
s-PP125	Tool for calibration	Boreholes PP125 open and PFL measured Boreholes PP127, PP129 closed	Characterisation of fracture
s-PP127	Tool for calibration	Boreholes PP127 open and PFL measured Boreholes PP125, PP129 closed	Characterisation of fracture
s-PP129	Tool for calibration	Borehole PP129 open and PFL measured Boreholes PP125, PP127 closed	Characterisation of fracture
c-PP125-1	Tool for calibration	Boreholes PP125 open and PFL measured Boreholes PP127, PP129 open	Characterisation of fracture
c-PP125-2	Tool for calibration	Boreholes PP125 open and PFL measured Boreholes PP127 open, Borehole PP129 closed	Characterisation of fracture
c-PP125-3	Tool for calibration	Boreholes PP125 open and PFL measured Boreholes PP127 closed, Borehole PP129 open	Characterisation of fracture
c-PP127-1	Tool for calibration	Boreholes PP127 open and PFL measured Boreholes PP125, PP129 open	Characterisation of fracture
c-PP127-2	Tool for calibration	Boreholes PP127 open and PFL measured Boreholes PP125 open, PP129 overpressure 2 bar	Characterisation of fracture

Name	Description	Boreholes	Purpose
c-PP129-1	Tool for calibration	Borehole PP129 open and PFL measured Boreholes PP125, PP127 open	Characterisation of fracture
TS-28 8	Forward/Prediction	KR14-18	
OL-KR38 NS	Forward	No Boreholes	Calculation of F-factor
OL-KR38 EW	Forward	No Boreholes	Calculation of F-factor
OL-KR24 NS	Forward	No Boreholes	Calculation of F-factor
OL-KR24 EW	Forward	No Boreholes	Calculation of F-factor
OL-KR48 NS	Forward	No Boreholes	Calculation of F-factor
OL-KR48 EW	Forward	No Boreholes	Calculation of F-factor

2.6 Task 7C

2.6.1 Modelling approach

The objective of this modelling task was the assessment and characterisation of the flow system in the near-field scale in Olkiluoto, Finland. In contrast with the site-scale and block-scale studies in Task 7A and 7B, respectively, describing the behaviour of only one fracture (Vidstrand et al. 2015) was targeted. Further objectives were the development of appropriate numerical DFN tools capable of handling the near-field in the presence of hydraulic disturbances as well as to gain insight into the advantages, drawbacks and limitations of this approach.

This task was subdivided into four subtasks (Vidstrand et al. 2015): Task 7C1 targeted the conceptualisation of a modelled area in the near-field scale, involving a single fracture of known position and transmissivity, as well as its immediate vicinity with boreholes in which single hole and hydraulic interference tests were performed. Task 7C2 was to develop a numerical model reproducing the behaviour of this area on the basis of the tests and also to predict its retention properties. Task 7C3 attempted to characterise the microstructure of the single fracture in the light of a measured flow distribution along the wall of a shaft created in the place of the boreholes that were used for the tests in Task 7C1. Finally, Task 7C4 assessed the uncertainties associated to the results.

Overall approach

The well tests conceptualised in Task 7C1 and actually implemented in the stochastic, three-dimensional, numerical DFN models of Task 7C2 helped characterise the overall system behaviour. The steady-state flow data was used to determine the mean transmissivity of the participating fractures. Building upon these experiences and considering a spatially distributed flow data set, in Task 7C3 a detailed analysis was performed through a series of two-dimensional models primarily targeting the microstructure of a single fracture. The problems were formulated in numerical models based on the finite element method solving the conventional flow equation

$$\nabla(T\nabla h) = 0$$

where

h is the hydraulic head [m] and

T is the transmissivity [m^2/s].

The analysis made extensive use of the versatility of the finite element method in defining arbitrary properties even cell-wise over the discretised domain, thus making feasible the assessment of highly heterogeneous fields. Retention properties of the medium of identified microstructure were estimated from the flow paths that resulted from the head solution.

The solution for head as well as for the pathlines and for the flow rates were calculated with the FEFTRA program package (Löfman and Mészáros 2013), which also served as a pre-processor to develop the numerical model.

The geometry of both the Task 7C1–C2 and the Task 7C3 problems suggested a near-radial flow, where the high head (sources) prevailed around the boreholes and the shaft, while the low head (sink) was assumed along the boreholes piercing and draining all the fractures along their path (Task 7C1–C2), as well as along the intersection line (a circle) of the shaft and the fracture at a depth of 235 m (Task 7C3). Thus the flow geometry was mainly defined by the location of the boundary conditions.

Since in Task 7C3 the focus of the modelling was the assessment of the fracture's behaviour, the most elaborated model input was the heterogeneous transmissivity distribution. In several attempts to reproduce this experiment with a series of numerical models, the focus of the modelling was the identification of the fracture's microstructure that is capable of bringing about the observed flow distribution at the shaft.

Mostly forward modelling was performed. Any inverse modelling was restricted to manual, albeit systematic trial-and-error adjustments of the input with no intention to apply a rigorous inverse modelling tool. In the course of the sensitivity analysis several input combinations were assessed in hundreds of stochastic realisations. An attempt was made to demonstrate the effect of the correlation length of the tranmissivity field on the flow and also to identify its value in comparison to the measured flows.

Besides the correlation length of the transmissivities also other sources of uncertainty played a significant role in defining the calculated flow distribution as well as the estimated retention properties of the media. When assessing the results it had to be recognised that they depend on some factors which do not make part of the conceptual model. These factors included inherent uncertainties of the input data as well as certain features of the numerical tools that produced some artefacts in the calculated results. The role of these factors will be discussed in details.

Data usage and interpretation

Task 7C1

In defining the external dimensions of the numerical models the information upon the extension of the full-head zone from the boreholes (15 m) was used (Vidstrand et al. 2015). The location and the geometry of the boreholes (Vidstrand et al. 2015) was honoured, albeit somewhat simplified in their transformation into vertical lines. Measured transmissivities at the intersections of the FR1 fracture and the PP1xx boreholes were applied to condition the transmissivity field over FR1. The datasheets on the background fracturing (Vidstrand et al. 2015) helped defining the DFN model, although detailed orientation data seemed to have been disclosed only about the KU1 boreholes. The calibration of the models was based on borehole flows from the single hole tests and the hydraulic interference tests, as well as on the calculated fracture transmissivities (Pekkanen 2009a, b).

Task 7C3

The flow was driven by the hydraulic gradient of exceptional magnitude induced by the KU2 shaft piercing the fracture of low transmissivity ($T = 10^{-9}$ m^2/s) at a level of $z = -235$ m, thus constituting a major sink in the system. The flow from the fracture that reached the shaft wall was regularly captured by a set of diapers carefully stuck over the circular intersection line of the cylindrical shaft and the planar fracture, from which the water was recovered and measured. The flow was thus integrated in time and its spatial distribution along the circle could be determined with reasonable accuracy.

The geometry of the problem was defined by the excavated shaft's dimensions in that the sink boundary conditions were prescribed along a circle of the shaft's diameter, as well as over the external boundaries of the model, where full head was assumed. The gradient between the prescribed high and low head boundaries was derived from the depth of the fracture.

Considering the properties of the microstructure of the model, no data supported anything other than a spatially correlated Gaussian transmissivity distribution. The correlation length as the associated parameter (T) field cannot be measured directly but may be deduced from observed flow properties, especially from the degree of channelization. This property affects flux distribution along a given line perpendicular to the flow, which, in the case of two-dimensional radial flow is a circle. Thus the flow distribution obtained from the shaft wall in the nappy experiment was informative with respect to the degree of flow channelization in the fracture, and consequently also to the value of the correlation length in the numerical model.

The mean of the transmissivity field was calculated from the geometric mean obtained at the former KU2 boreholes. The spread and the correlation length were calibration parameters. The standard deviation of the log-transmissivites ranged from 0.0 to 2.8 m^2/s in the simulation. Correlation length ranged from 0.1 to 3.0 m. The fracture was not intersected by another one inside the modelled domain.

The manual calibration of the model was based on the systematic comparison of the observed and calculated peaks of flow at the shaft wall. Some information suggested that the southwestern wall of the shaft was partly covered with an unknown amount of grout powder, effectively rendering the shaft wall partially closed for flow. The effect of this circumstance was studied with a sensitivity case.

2.6.2 Conceptual model

The three three-dimensional conceptual models of Task 7C1 comprised (1) the identified fracture denoted FR1 of known location and properties, (2) a set of stochastic fractures described statistically on the basis of the available data, as well as (3) the three groups of boreholes in places of the would-be shafts, also giving names to the Task 7C1 submodels (see Figure 2-2 below):

- KU1 submodel / shaft: boreholes PP131, PP134 and PP137.
- KU2 submodel / shaft: boreholes PP122, PP123, PP124, PP126 and PP128.
- KU3 submodel / shaft: boreholes PP125, PP127 and PP129.

The two-dimensional conceptual model of Task 7C3 only contained the FR1 fracture with a stochastic transmissivity field over it and the boundary conditions inducing near-radial flow towards the shaft.

Main assumptions and simplifications

Task 7C1

The Task 7C1 conceptual models consisted of deterministic and stochastic entities. Deterministic elements were the FR1 fracture, the three sets of boreholes and the observed transmissivities of the FR1 fracture at the boreholes. Stochastic entities comprised all the other fractures, which were input as their statistical description into the models, and the transmissivity field assumed over the FR1 fracture following a spatially correlated Gaussian distribution. Following from this setup the boundary conditions were both deterministic (along the perimeter of the deterministic FR1 fracture and the prescribed drawdowns at the open boreholes) and stochastic (along the stochastic fractures at the external boundaries of the model). All fractures were considered planar and connected to each other along their intersection lines. The FR1 fracture was set horizontal in all the three submodels (KU1, KU2 and KU3). All boreholes were set vertical somewhat disregarding their given, slightly curved path. Boreholes piercing the deterministic FR1 or the stochastic fractures were also connected to them hydraulically. Open boreholes were modelled with a prescribed constant head boundary condition equal to the measured drawdowns, whilst closed boreholes acted through the effect of their interconnecting the pierced structures by their high conductance. No correction was performed during the post-processing with regard to the shape of the depression zone upon the assumption that the resolution of the discretisation in the numerical model would be adequate to follow the depressed head field with sufficient accuracy.

The generated transmissivity distribution, besides being stochastic by nature, also included the measured values at fixed locations of the boreholes (conditioning). The fixed values were incorporated in the transmissivity field using the same correlation length, similarly as suggested by Dietrich and Newsam (1996) so as not to break the internal structure of the distribution (Figure 2-1).

These simplifications served the purpose of efficiently and quickly building numerical models in numerous realisations from the conceptual models. In addition, the development of numerical tools capable of doing so was one of the objectives in Task 7 in general, aiming their subsequent deployment in other projects as well.

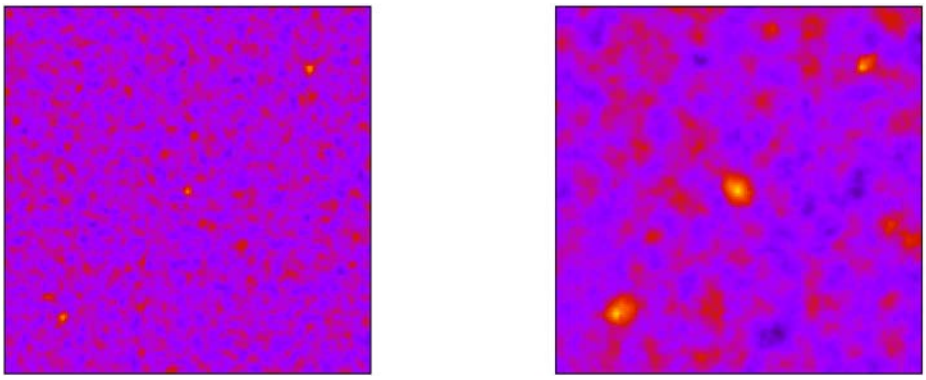

Figure 2-1. *Illustration of conditioning the spatially correlated Gaussian field on observations placed along the diagonal of the quadrat. Left: smaller correlation length. Right: larger correlation length.*

Task 7C3

Flow was assumed to remain in the fracture, i.e. the modelling domain was assumed two-dimensional. In order to optimally assess the role and the behaviour of the micro-structure of the single fracture, the following was assumed:

The fracture was considered planar and completely horizontal. In contrast to this, data confirmed that neither of this assumption was actually true, but in the presence of the large hydraulic gradient between the surface and the fracture exposed in the shaft the significance of these deviations could be ignored.

The relevant hydrogeological property of the modelling domain was the transmissivity and its distribution. Though there must have been several geological, hydrogeological and geochemical processes contributing to the formation of the fracture's microstructure (cracking, clogging, accumulation of allochthonous and autochthonous clay, appearance of precipitates, etc) and shaping its properties relevant to the flow – but none of these factors or a set of these factors had been identified as the primary agent. In the lack of such information we assumed that the weight of contributing factors was more or less similar. It followed from this assumption that regarding the central limit theorem the distribution of the transmissivities had to be expected spatially correlated Gaussian, which was defined by the mean, the standard deviation and the correlation length as its characteristic properties.

Geometrical description

Task 7C1

The three submodels' external boundaries were those of a straight prism around the actual sets of boreholes. The vertical length of the modelled area was 40 m and laterally it extended to the distance of 15 m from the boreholes where already full head was attained during the tests (Vidstrand et al. 2015). The deterministic, horizontal FR1 fracture intersected the modelled area at its middle.

The rest of the fractures were added as a Discrete Fracture Network (DFN) component to the model, in which the stochastic fractures were assumed circular with the necessary attributes (centre, orientation, radius and transmissivity) and approximated with a regular hexagon. The parameters (fracture intensity, orientation and the concentration parameter κ of the von Mises-Fisher distribution) defining the DFN models were derived partly from fracture data of the KU1 submodel. The P_{32} fracture intensities were taken as the Terzaghi-corrected P_{10} intensities. Since no orientation data was available for the KU2 and KU3 submodels, the same parameters were used also therein. However, fracture intensities had to be reduced significantly for the KU3 submodel to limit flow from the perimeter of the modelled area to the boreholes (see the Discussion for an elaboration on this). Parameters for the von Mises-Fisher orientation distribution (dip, dip direction and κ) were calculated with the R statistical software's CircStats (Lund and Agostinelli 2010) and VecStatGraphs3D (Felicismo et al. 2011) packages, respectively (Table 2-1).

The size distribution was not based on any hard data though: It followed from the fracture intensities that only a handful (5–10) of stochastic fractures were generated in each realisation and in order that they would participate in a meaningful way in the model (i.e. they would be connected to one of the boundary conditions) their size was set large enough to reach the model boundaries. Smaller floaters disconnected from each other and from the boundaries (including clusters of them) were removed from the model during preprocessing, whilst too large fractures would have exhausted the given fracture intensities already in small numbers. The size distribution was set to follow truncated power-law:

$$r = r_{\min}(1 - r_L)^{b-1}$$

where

$r_{\min}$ is the lower bound of the fracture size,

b is the normalising constant, and

r_L expresses the truncation.

The transmissivity distribution was set to depend on the size of the fractures (parameter S_L^i) giving larger fractures a more significant role in the model (see Section 1.6.2 for a detailed description on this correlation).

Table 2-1 Parameters of the DFN submodels.

Parameter	KU1	KU2	KU3
Dip	26.0	26.0	26.0
Dip direction	60.0	60.0	60.0
von Mises-Fisher κ	21.9	21.9	21.9
P_{32}	0.11	0.11	0.01
r_{min}	10.0	10.0	8.0
b	2.5	2.5	2.5
r-T dependence S_L^i	0.1	0.1	0.1

Task 7C3

The modelled area was a horizontal plane defined at the depth of the FR1 fracture, and comprising a domain of a 30 m × 30 m quadrat centred around the shaft of 3.5 m diameter. When meshing this domain area two types of finite elements were used: either regular quadrats of size 0.3 m or right angle triangles obtained by further splitting these quadrats along one of their diagonals. Both the quadrats and the triangles were linear finite elements in terms of their basis functions. Results were calculated with both types of discretisation to see the effect of these schemes.

The true geometry of the problem, however, was not rectangular like that of the underlying finite element mesh, but circular. The unnecessary parts of the rectangular mesh (i.e. the corners of the quadrat and the internal shaft area), although being present in the calculations, were effectively clipped off by the circular boundary conditions.

In modelling the flow field, no intersection with other fractures was considered. By the time the shaft was excavated from below, the rock volume around the boreholes that participated in Task 7C1 had been removed and no other boreholes were taken into account, either.

Processes considered

Task 7C1

The dataset available for the TaskC1 subtask facilitated a certain level of understanding of the flow system in the near-field scale. The magnitude of the drawdowns and the induced outflows in the single-hole tests as well as in the hydraulic interference tests allowed the estimation of the *mean transmissivity* of the fractures, however, it was not possible to derive any insight about the microstructure of the FR1

fracture. Thus, with the drawdowns at the given setups characteristic to the performed tests, the simulations targeted the determination of the borehole flows in multiple realisations. The calculated flows were used for the characterisation of the fractures in terms of their mean transmissivity.

Besides the head gradient and the transmissivities, the flow distribution was also affected by the presence of boreholes (both open and closed), thus the boreholes had to be considered and included in the model the way as they interacted with both the deterministic and the stochastic components.

Task 7C3

The behaviour of the flow was assessed through a series of steady-state simulations targeting head, as well as its gradient and the flow paths, which developed in the FR1 fracture between the high and low head boundaries. As the head difference could be measured with relatively high accuracy this input was not varied. Both the head and the flow distributions depended on the properties of the actual transmissivity field (mean, spread and correlation length of the spatially correlated Gaussian distribution). Compared to Task 7C1, a distinctly different, additional information in this subtask was the measured, exiting flow distribution along the shaft wall at the intersection of the FR1. This data provided further insight into the flow system and facilitated the estimation of the correlation length. The role of these inputs was assessed in several realisations.

Thus the primary agents that shaped the flow field were the large head gradient and the assumed transmissivity fields with its properties.

Boundary conditions

The role of the boundary conditions was to connect the model to the outside world and thus define the main direction of flow inside the numerical representation of the fracture(s) and the borehole(s).

Task 7C1

Based on the information that full head was attained already at a distance of 15 m from the open boreholes (Vidstrand et al. 2015), which brought about the large drawdowns along the vertical axis of the modelled volume, no-drawdown was prescribed over the lateral boundaries of the modelled volume. In the case of DFN models, in practice this meant that all the fractures were clipped at a distance of 15 m (measured along the horizontal x and y coordinate axes) from the vertical centre of the model, and along the clipped edges extending as far as the lateral boundaries no-drawdown was prescribed. This boundary acted as the source of water.

The PP12x and PP13x boreholes, which participated in the single-hole tests and in the hydraulic interference tests were all about 100 m in length. It is believed that during the tests these boreholes induced flows perpendicular to them both in the rock and in the pierced fractures, implying that the flow parallel to these boreholes was small, at least to the extent that it could be ignored. Thus the top and bottom faces of the 40 m long prisms (i.e. those perpendicular to the boreholes) were considered closed for the flow.

The sink(s) in the model was/were implemented using the open boreholes close to the vertical centre of the model, and they were represented by prescribing the measured drawdowns (KU1: 183.52 m, KU2: 187.09 m and KU3: 182.81 m) at the open borehole(s). The closed boreholes were connected neither to the sources nor to the sinks directly, but, similarly to fractures falling completely inside the model, added to the connectedness of the model.

Task 7C3

In the nappy experiment the main direction of the flow pointed towards the shaft from around its environment. Head in the bedrock at a distance of 15 m from the shaft could be considered already undisturbed, thus the source of water was assumed as a no-drawdown boundary (h = 0 m constant head) at 15 m from the centre of the shaft. The effect of the shaft, i.e. the sink in the model was represented by constant head (h = −235 m) distributed along a circle of 3.5 m diameter.

2.6.3 Model implementation

All the models were created and solved with the FEFTRA program package developed by VTT/ Posiva (Löfman and Mészáros 2013). Simulations for the Task 7C2 and Task 7C3 subtasks were based on the DFN paradigm and the finite element method. As the models involved stochastic input also their results were stochastic, of which the mean was considered in the calibration process.

Numerical model(s)

Task 7C2

The KU1, KU2 and KU3 conceptual models developed in Task 7C1 served as bases for the simulations performed in this subtask. Each sub-model was assessed in a few simulations testing various combinations of parameters, resolution and boundary conditions. Each simulation was performed in typically 20 realisations. In each realisation the input parameters for a given sub-model defined the creation of and solving the numerical models in three distinct phases.

First, a spatially correlated Gaussian distribution was developed for the FR1 fracture given its mean, standard deviation and correlation length as well as the locations of the observations used for conditioning (this step was performed by the FEFTRA/davja program module). Secondly, the FR1 fracture was discretised into finite elements (element size uniformly 0.18 m) with the same resolution as that of the Gaussian T-field, then the discretised stochastic fractures and the boreholes were added (this step was performed by the FEFTRA/vintage program module). This step also included the development of hydrogeological properties for all participating entities and then their assembly into a single model: the properties of the FR1 zone were read in from the pre-generated T-field, the transmissivities of the stochastic zones were chosen from the given truncated lognormal distribution and the conductance of the boreholes was set as given in the inputs. In addition to the finite element mesh and its properties the boundary conditions were developed in this phase as well (Figure 2-2). Thirdly, the numerical model was solved and post-processed to produce the head and flow distribution (this step was performed by the FEFTRA/solvit program module).

Task 7C3

Similarly to the Task 7C2 simulations, modelling the Task 7C3 subtask was also performed in three steps of nearly identical functionalities, however, the second phase responsible for the mesh generation and pre-processing in general was performed with the FEFTRA/mk2dmesh program module complemented with a few ad-hoc utilities. It follows from the conceptual model of this subtask that the modelled two-dimensional domain was simpler (only one fracture and no boreholes). The element size was 0.06 m (both linear rectangles and triangles were used – see details below).

Parameters

Since in the mathematical model transmissivity was the only parameter in the strict sense, this section only refers to parameters defining the transmissivity distribution. Other inputs affecting the connectivity between the boundary conditions were treated in the section on Geometrical description.

Task 7C1

Stochastic fractures were considered homogeneous with respect to their transmissivity. The transmissivity value for each fracture was chosen from a truncated lognormal distribution, of which mean was a calibration target

$$-13.0 \le \lg T \le -10.0$$

with a final value of $\lg T = -12.5$ m^2/s, while its standard deviation $\sigma = -0.6$ m^2/s was calculated from the data disclosed in the Task 7C deliverables. Besides being lognormal, the transmissivities of the stochastic fractures were set semi-correlated to their size (see section Geometrical description).

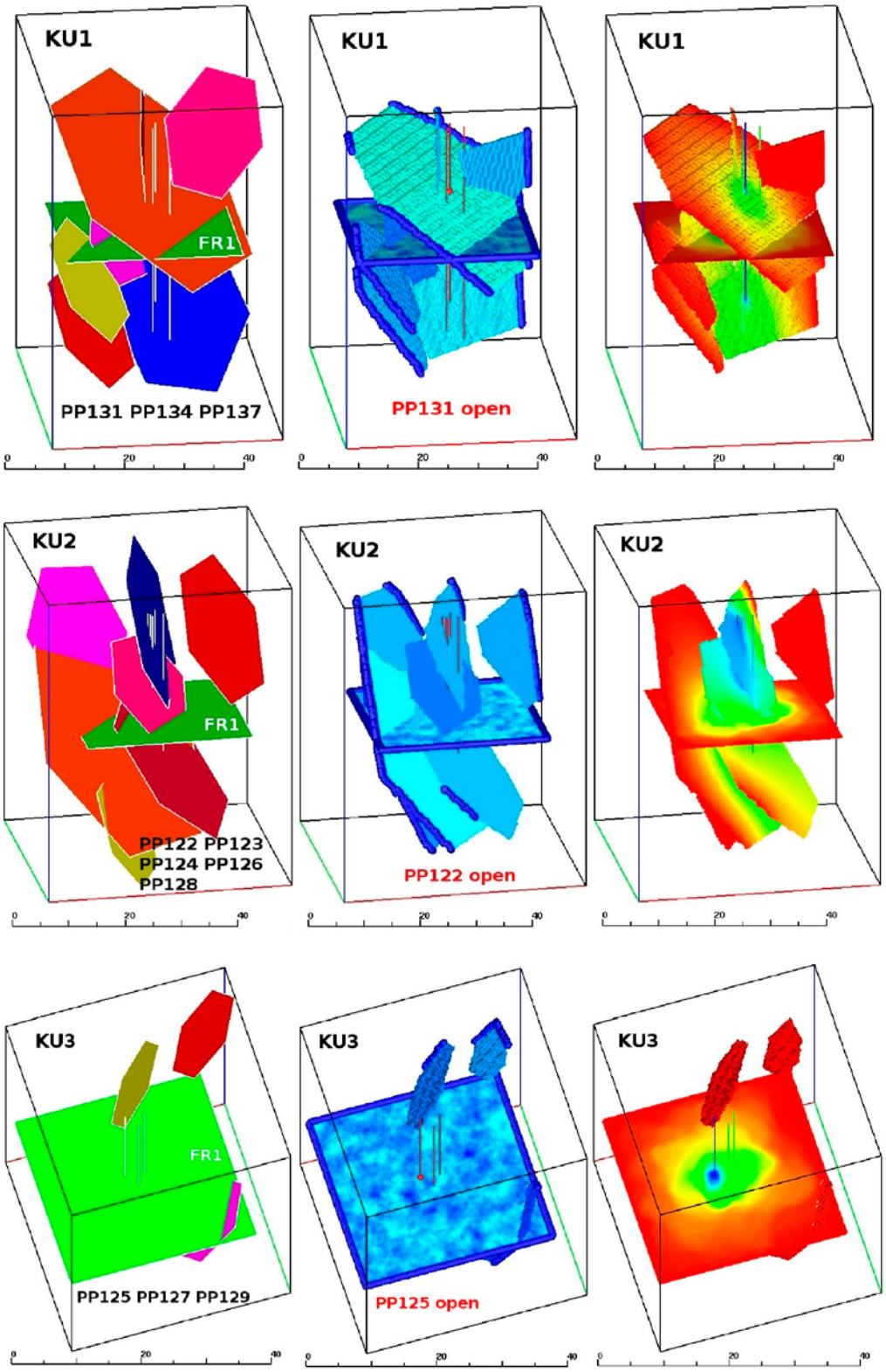

Figure 2-2. *Conceptual (left column) and numerical (middle column) models, as well as solutions (right column) in the single- and cross-hole test submodels. No-drawdown boundary conditions are indicated with blue, drawdowns with red bubble in the numerical models.*

Task 7C1 and Task 7C3

The deterministic FR1 fracture was assumed heterogeneous with respect to its transmissivity. In the lack of any specific information on the genesis of the fracture, the lg(T) field was defined spatially correlated Gaussian.

Algorithms capable of creating a spatially correlated Gaussian field are usually implemented either employing the spectral approach using Fast Fourier Transform (see, e.g. Ruan and McLaughlin 1998) or are based on some variants of matrix factorisation (see, e.g. Dietrich and Newsam 1996). This study was based on the latter, with the provision for honoured values at the locations of the observations (conditioning). Using this technique with a matrix of size identical to that of the finite element mesh would have rendered the creation of the transmissivity field computationally more expensive than solving the model itself, thus for the sake of efficiency the size of the factorised matrix did not extend to the full size of the finite element mesh but the modelled area was covered with a lattice of overlapping, smaller matrices. The optimal size (optimal in terms of computational efficiency) of these matrices was determined experimentally.

Correlation length was a calibration parameter in Task 7C3 with the conclusion that the results may suggest correlation lengths beyond 2.0–2.5 m. On the basis of these results in the Task 7C1 simulations the correlation length was assumed 16 cells, i.e. 2.9 m.

Model conditioning and calibration

Task 7C1

The transmissivity fields of the FR1 fracture honoured the measured values at the boreholes that were used in the hydraulic tests in all the three submodels (KU1, KU2 and KU3). Thus conditioning the T-field at the disturbances was not employed as a measure to control the flow, but to build a model that makes use of this information as well.

Both the single hole tests and the hydraulic interference tests were used for the calibration, except for the c-PP127-2 test in which a 2 bar overpressure was applied. Those interference tests in which all the three boreholes (c-PP125-1, c-PP127-1 and c-PP129-1) were open and in the field the flows were measured in different boreholes, were unified into a single simulation in which the flows were determined for all the three open boreholes.

The geometric mean of the measured transmissivities served as an initial value for the calibration of the mean of the T-field. No formal or automatic procedure was used in the calibration, but a manually performed, systematic trial-and-error method attempted to find a single optimum mean for all the three submodels instead. Each calibration step involved the assessment of twenty realisations.

Task 7C3

As this subtask targeted the characterisation of the microstructure of the FR1 fracture, the role of all the three parameters of the spatially correlated Gaussian transmissivity field was assessed. Of these the calibration of the correlation length has become feasible making use of the flow distribution along the shaft wall, as it was believed of diagnostic value with respect to the channelisation of the flow.

2.6.4 Results

Task 7C1

The required performance measures for this subtask were the parameters describing the conceptual model. Besides the geometrical description (see above) the transmissivity distributions are presented in Table 2-2 as either calibrated (mean) or assumed (standard deviation and correlation length) values. In the light of the measured borehole flows it had to be assumed that the vicinity of the KU3 shaft area is significantly less conductive than the KU1 and KU2 area. Because of this the three submodels could only be described with different transmissivity distributions.

Note that the mean and the standard deviation of the *T*-field are attributes to both of the spatially correlated Gaussian distribution over the deterministic FR1 zone and of the lognormal distribution

of the stochastic fracture's transmissivities. Although the two distributions are independent – in the absence of data indicating otherwise – their corresponding parameters were set equal in the same submodel.

Table 2-2. Parameters of the transmissivity distributions in the three submodels.

parameter	KU1	KU2	KU3
μ(lg(*T*)) [m²/s]	−10.5	−10.5	−12.5
σ(lg(*T*)) [m²/s]	0.6	0.6	0.6
Correlation length [m]	2.9	2.9	2.9

Task 7C2

The performance measures of this subtask are the actual results of the simulations carried out using the conceptual models defined in Task 7C1. Results include head, flows and retention properties expressed in terms of statistics of F-factors defined as the double of the *wl/q* quantity. Note that instead of the method based on the breakthrough curves the *wl/q* properties were integrated along the pathlines. The calculated mean and the standard deviation of the log-F-factors are presented (Table 2-3) for the submodels (20 realisations, 100 pathlines/realisation for the six F-factor submodels).

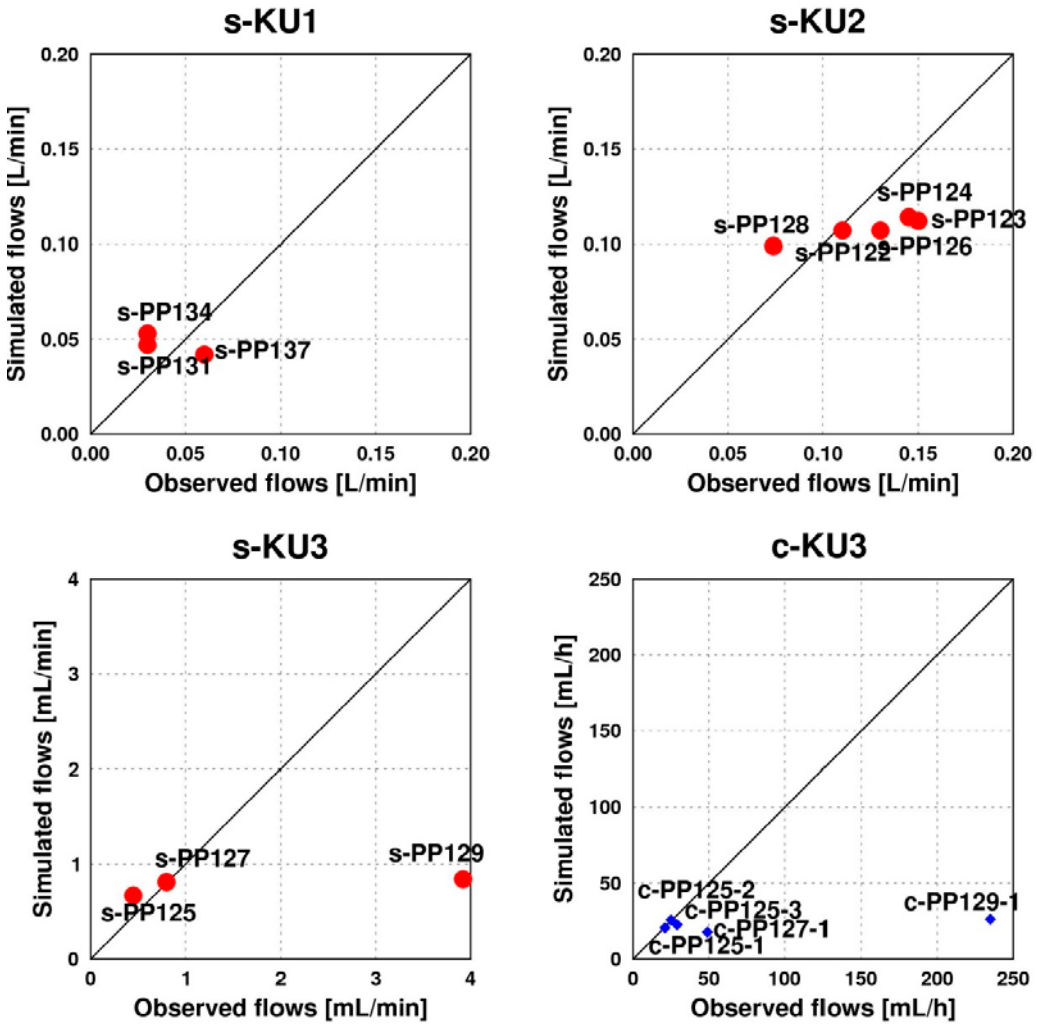

Figure 2-3. *Comparison of observed and simulated flows in the single-hole (s-) and cross-hole (c-) tests. The results are presented in the same unit as they were reported (Pekkanen 2009a, b).*

Hydraulic head

In the 11 single hole tests and 5 cross-hole tests the head fields varied between the fixed boundary conditions and together with the transmissivity fields served as a basis for the flow calculations. Three examples are presented (Figure 2-2) in connection with the conceptual and the numerical model (also showing the transmissivity fields over the fractures and the boundary conditions) of a certain realisation. Further, a head distribution used for the F-factor calculation is also shown (Figure 2-4). Note that because of the distinctly different magnitudes of the hydraulic gradient in the models that calculated the well tests and the F-factors (cca 12 m/m and 0.1 m/m, respectively), the variability of the head field is much greater in the latter.

Borehole flows

The flow magnitudes at the boreholes were calculated directly from the solution of the finite element method and averaged over 20 realisations. While most of the tests could be reproduced within the targeted order-of-magnitude approximation, both the single-hole and the cross-hole tests suggest that in the reality the PP129 borehole is better connected to the boundaries (Figure 2-3) than in the numerical models. This connection may manifest itself in various ways: either the FR1 fracture is more transmissive between the model boundaries and the PP129 borehole, or this borehole is connected at a different depth from that of the FR1 zone to the sources.

Retention properties (F-factors)

In order to calculate the retention capabilities of the media in the specified north-south and east-west directions at the given 0.1 m/m hydraulic gradient, the boundary conditions were re-set for the submodels, all boreholes were removed (nonetheless, the Gaussian T-field remained conditioned at the observations) and the head recalculated in at least 20 realisations. In each realisation 100 particles were released into the flow field and the *wl/q* quantity was integrated along their paths to the sinks (Figure 2-4). The pathlines were calculated with the particle tracking algorithm implemented in the FEFTRA program package.

The F-factor values were taken as the double of *wl/q* at the destination of the particles. In the light of the calculated statistics on the lg(*F*-factor) values, in accordance with the expectations the retention is greater around the KU3 area (Table 2-3).

Table 2-3. Mean and standard deviation of F-factor values in the three submodels calculated from populations of n=2 000.

Model	μ(lg(*F*)) [yr/m]	σ(lg(*F*)) [yr/m]
OL-KR24_NS (KU1)	8.69	0.97
OL-KR24_EW (KU1)	8.70	0.93
OL-KR38_NS (KU2)	8.75	0.96
OL-KR38_EW(KU2)	8.78	0.94
OL-KR48_NS (KU3)	10.77	1.01
OL-KR48_EW (KU3)	10.78	0.94

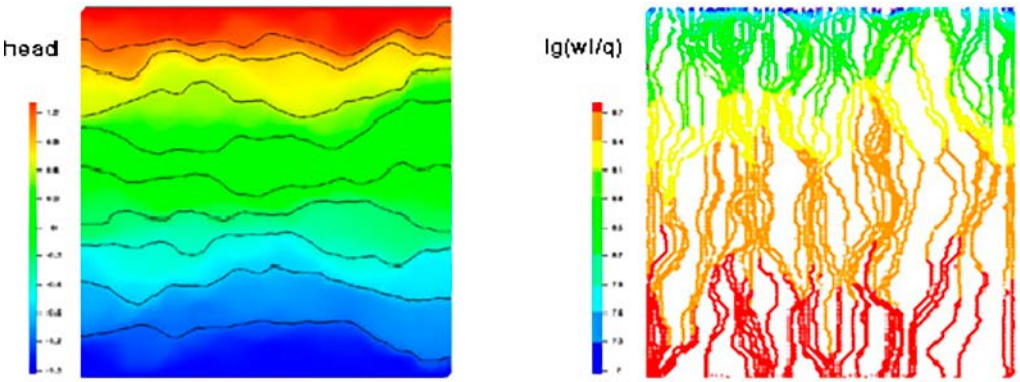

Figure 2-4. *Retention in the calibrate media. Left: hydraulic head. Right: lg(wl/q).*

Task 7C3

The performance measures were the comparison of the measured and simulated flows at their exit from the FR1 fracture into the KU2 shaft which was created in the place of the PP122, PP123, PP124, PP126, PP128 and the OL-KR38 boreholes. These results were re-calculated with several input parameter combinations and over many realisations to understand and assess their role in the flow distribution, of which one of the most successful is presented (Figure 2-5). Note that with the circular boundary conditions the exact location of the flow peaks cannot be influenced. The properties of the transmissivity distribution, however, can exercise control on the degree of channelization of the flow and thus also on the magnitude and number of flow peaks.

Task 7C4

The performance measures are the quantified factors contributing to the uncertainty of the results. In the following several such factors are listed, of which significance in comparison with the others is difficult to judge, thus the ordering of this list can be considered random.

Arithmetic precision (single and double precision flow field)

It can be shown that pathlines, and consequently also retention properties calculated from the same input, but using different precision in the representation of floating-point numbers will lead to markedly different results (Figure 2-6).

The variability of results obtained from calculations performed with different precision may reach those obtained from different realisations.

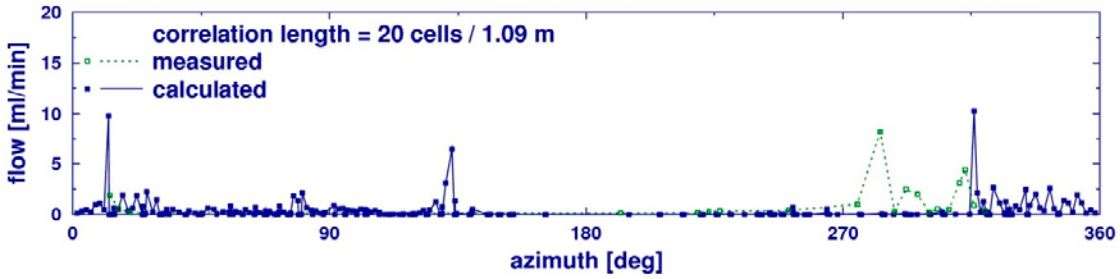

Figure 2-5. *Distribution of measured and simulated flow along the shaft wall.*

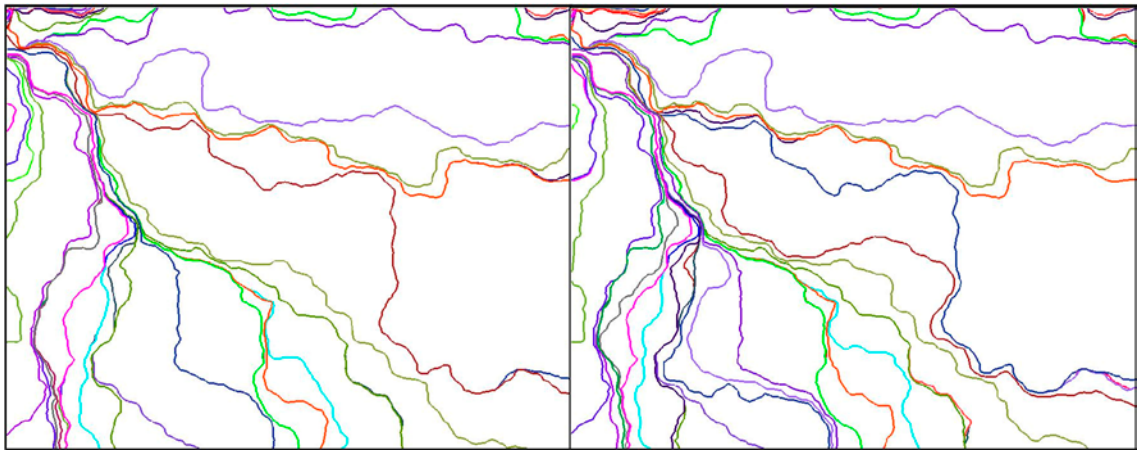

Figure 2-6. *Pathlines traversing head fields obtained from single (left) and double precision (right) calculations in the vicinity of the shaft in Task 7C3.*

Flow pattern (degree of channelization) vs. correlation length

With the increase of the correlation length the extension of zones with more or less similar transmissivities increases: wider flow routes develop among larger "islands", which are only moderately or not visited by the flowpaths (Figure 2-7. At higher correlation lengths some particles are bound to encounter less obstacles towards their destination (the sinks).

Darcy velocity distribution vs. correlation length

The geometric concentration of the above flow patterns is coupled with higher velocities as well (Figure 2-8). It has been observed elsewhere that on the longer run the hydraulic conductivity of discharge zones increases, which may or may not be counterbalanced by the decreasing hydraulic conductivity of the recharge zones.

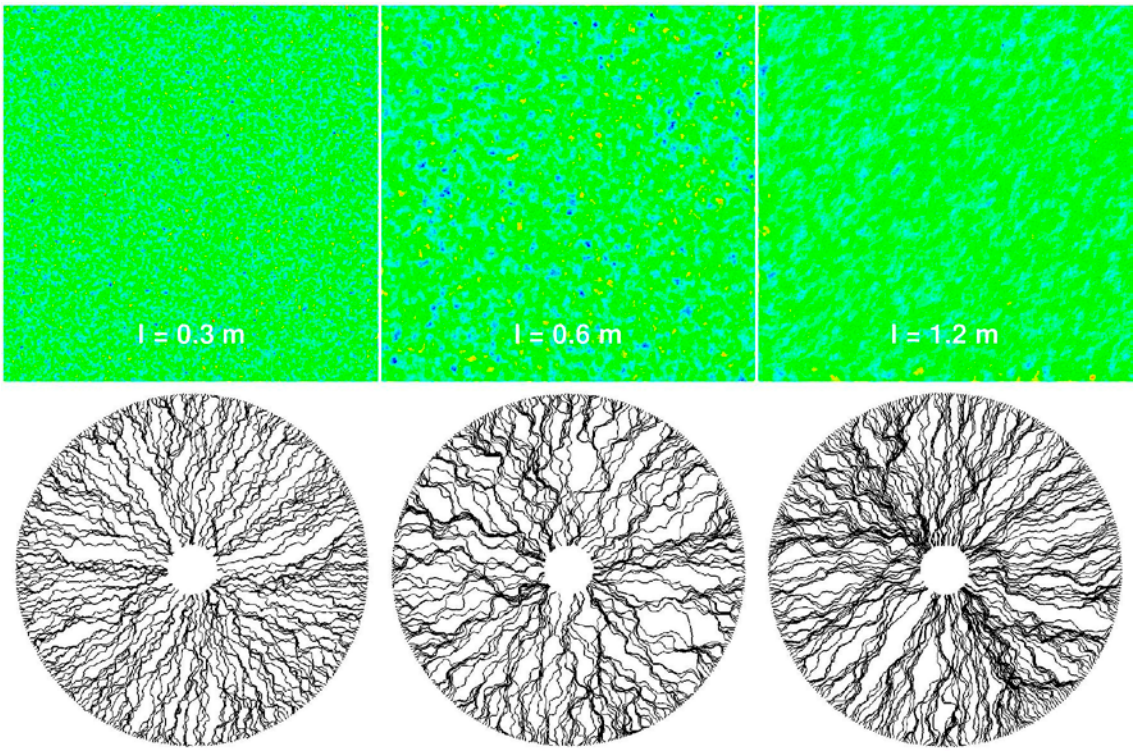

Figure 2-7. *Distribution of flow paths at correlation lengths of 0.3, 0.6 and 1.2 m. σ(lg(T)) = 1.0 in all the three cases.*

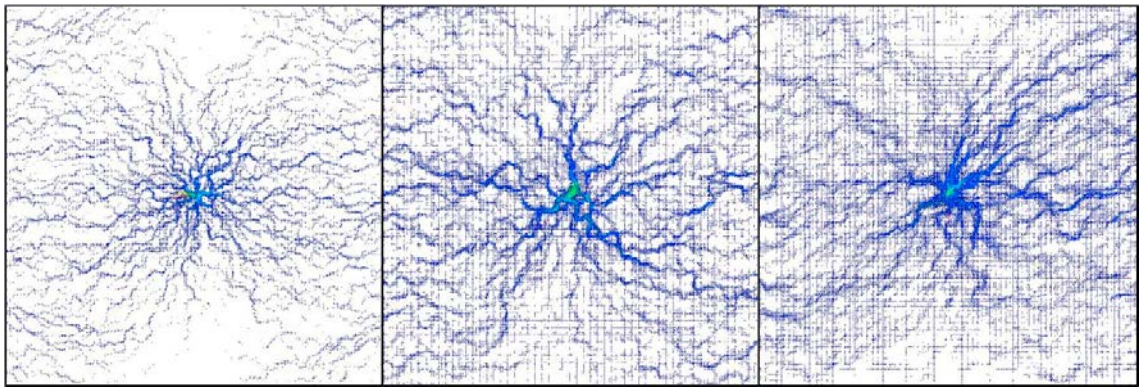

Figure 2-8. *Distribution of Darcy velocities at correlation lengths of 0.3, 0.6 and 1.2 m.*

Flow distribution at the shaft wall as a function of the correlation length

The flow patterns and the velocity distributions above suggest that the flux crossing any given line or surface perpendicular to the flow would exhibit a non-uniform distribution. The degree of non-uniformity is a function of the factors responsible for the channelization of the flow. This non-uniformity was actually measured at the shaft wall and also compared to flow data extracted from the simulations along the intersection of the shaft wall (a perpendicular surface to the radial flow). It is demonstrated that the increasing correlation length contributes to the non-uniformity of the flow (Figure 2-7 and Figure 2-9).

Note that even if the (geometric) mean transmissivity is identical in the three presented cases, the effective transmissivity and thus the total flow is not guaranteed to be equal if the correlation length is different. In case a low-transmissivity zone or "ring" develops in one of the realisations between the sources and the sinks (i.e. more or less perpendicular to the main direction of the velocities), then the total flow would necessarily be smaller than if the low-transmissivity areas are disrupted or the flow takes place in a less variable field.

However, experiments were unable to reveal a conclusive evidence for a monotonic or even just a trend-like dependence between the correlation length and the number of peaks (where a "peak" would be considered to be a local maximum and rising above a certain threshold, e.g. 2 ml/min).

Spread of the transmissivity

Another factor that contributed to the development of non-uniform flow patterns and to the variability of the total flow was the spread of the values in the transmissivity field. With the correlation length fixed at 0.5 m (9 cells) different Gaussian fields were generated with standard deviations of $\sigma_1(\lg(T)) = 0.4$ m^2/s, $\sigma_2(\lg(T)) = 1.0$ m^2/s and $\sigma_3(\lg(T)) = 1.8$ m^2/s, which resulted in strikingly different flow patterns (Figure 2-10). See the Discussion for further comments on this.

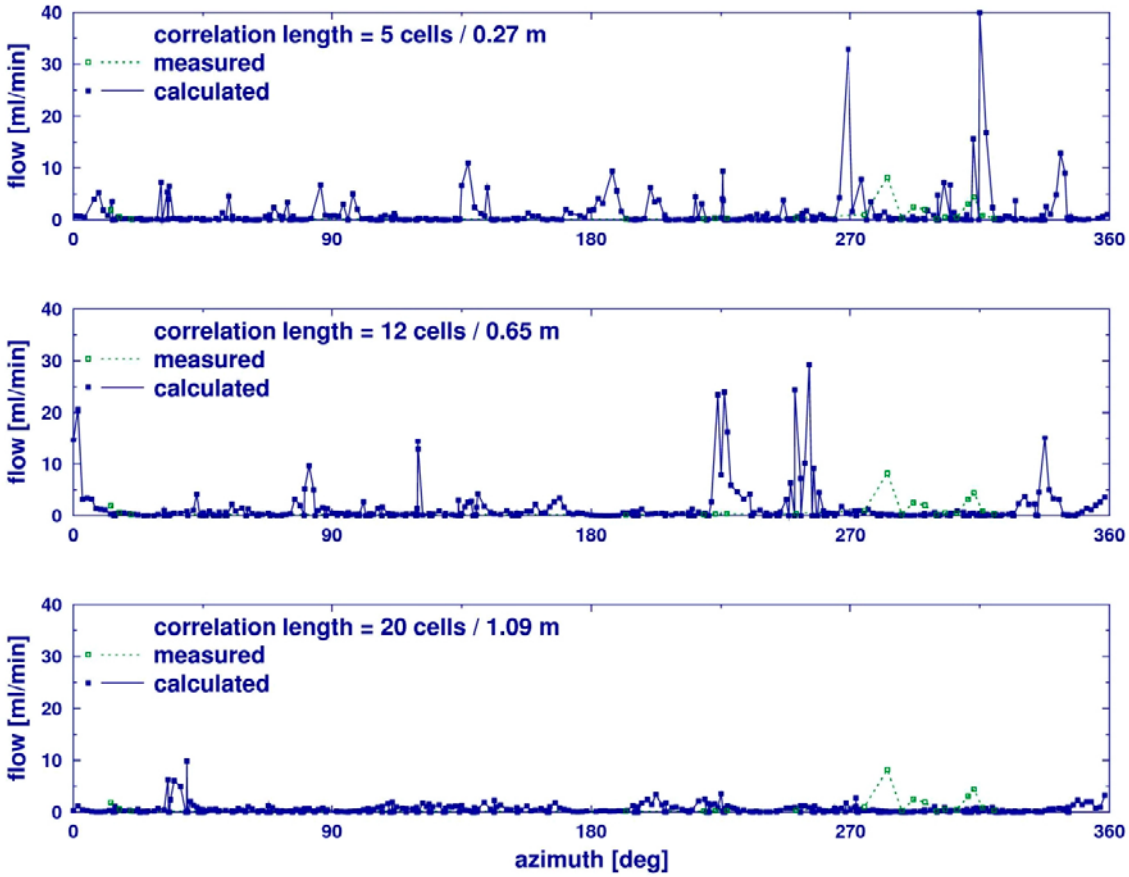

Figure 2-9. *Flows at the shaft at correlation lengths of 0.3, 0.6 and 1.2 m.*

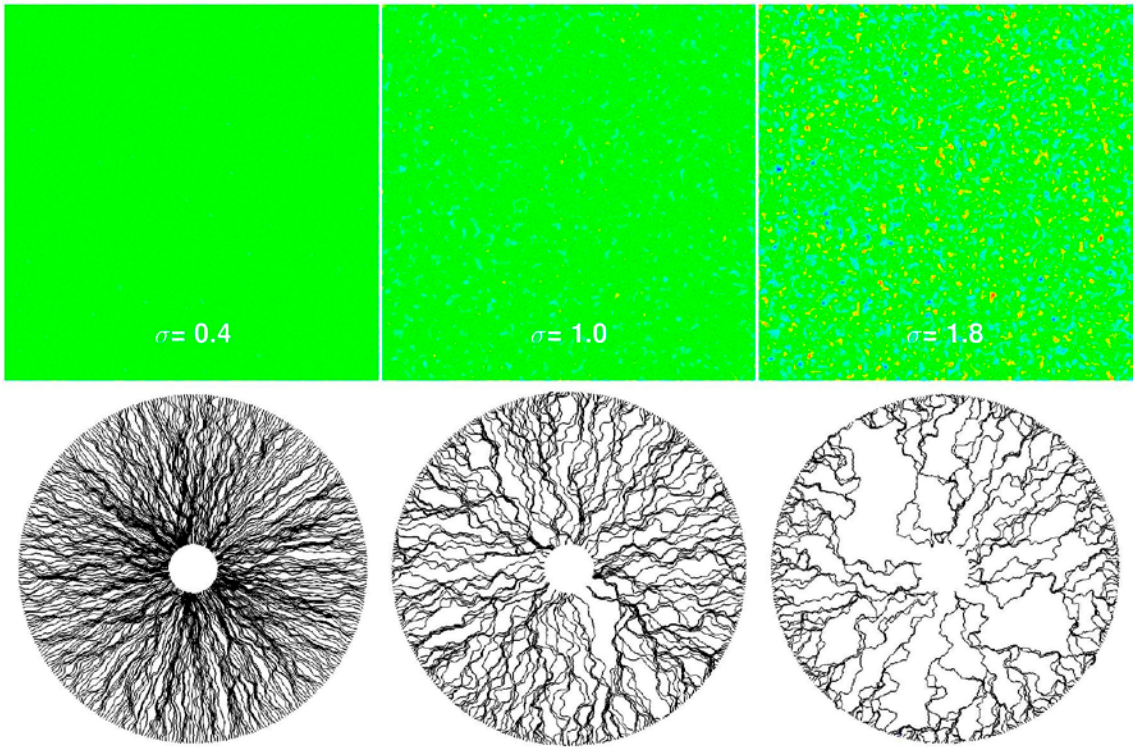

Figure 2-10. *Flow patterns at different spread of the transmissivity field.*

Dependence of the retention properties on the correlation length

The magnitude of the correlation length can be estimated in several ways, however, independently from the method used for the estimation of autocorrelation at some scale, the obtained value influences flow via channelization. With the increase of the correlation length the spread of the calculated F-factors increases too (Figure 2-11), of which consequence is that the frequencies in the ranges of the smaller values will determine the retention of the media from the practical point of view.

Discretisation pattern vs. calculated retention properties

It can be shown that certain results are sensitive to the algorithms which are used for their creation. When the conceptual models are converted into numerical models, which are bound to be solved with a specific method, results will depend on the attributes and limitations of these algorithms.

Some of the finite element methods, including the Galerkin approximation which has been implemented in FEFTRA, access the discretised domain via the integration points used in the Gaussian quadrature (Figure 2-12). Since the various discretisation schemes make use of different finite element libraries, the distribution of the integration points and the accuracy of the numerical integration is different in each scheme. We show that when advection is a dominant process the possible alignment of the finite element mesh with the underlying structure of the integration points has an effect on the results (Figure 2-13 and Figure 2-14).

Note that the two results were obtained from identical conceptual model and inputs. Variability of the results obtained from the two discretisation schemes may be on a similar order of magnitude than the variability among different realisations of a stochastic model.

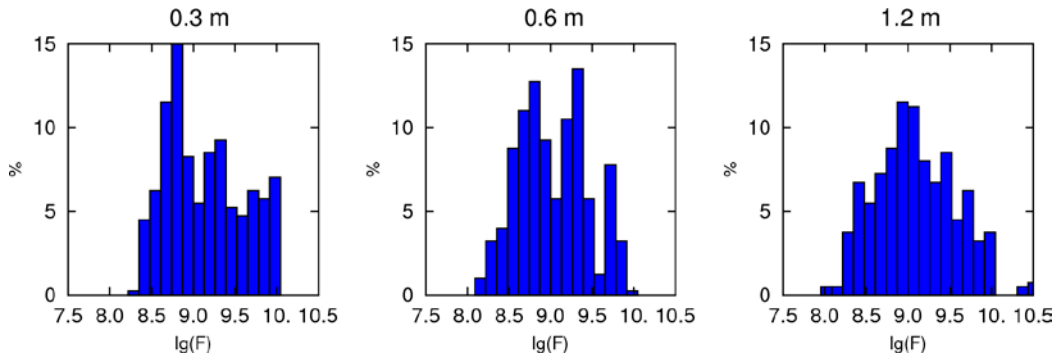

Figure 2-11. *F = 2 wl/q frequencies for correlation length of 0.3 m, 0.6 m and 1.2 m, respectively. As the correlation length increases, the frequencies of smaller F-values grow indicating channelization and poorer retention.*

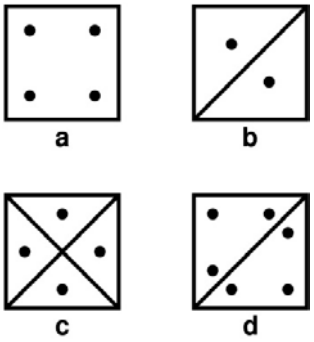

Figure 2-12. *The distribution of integration points when discretising the unit quadrat with different types of finite elements. a) one linear quadrat b) two linear triangles c) four linear triangles d) two quadratic triangles.*

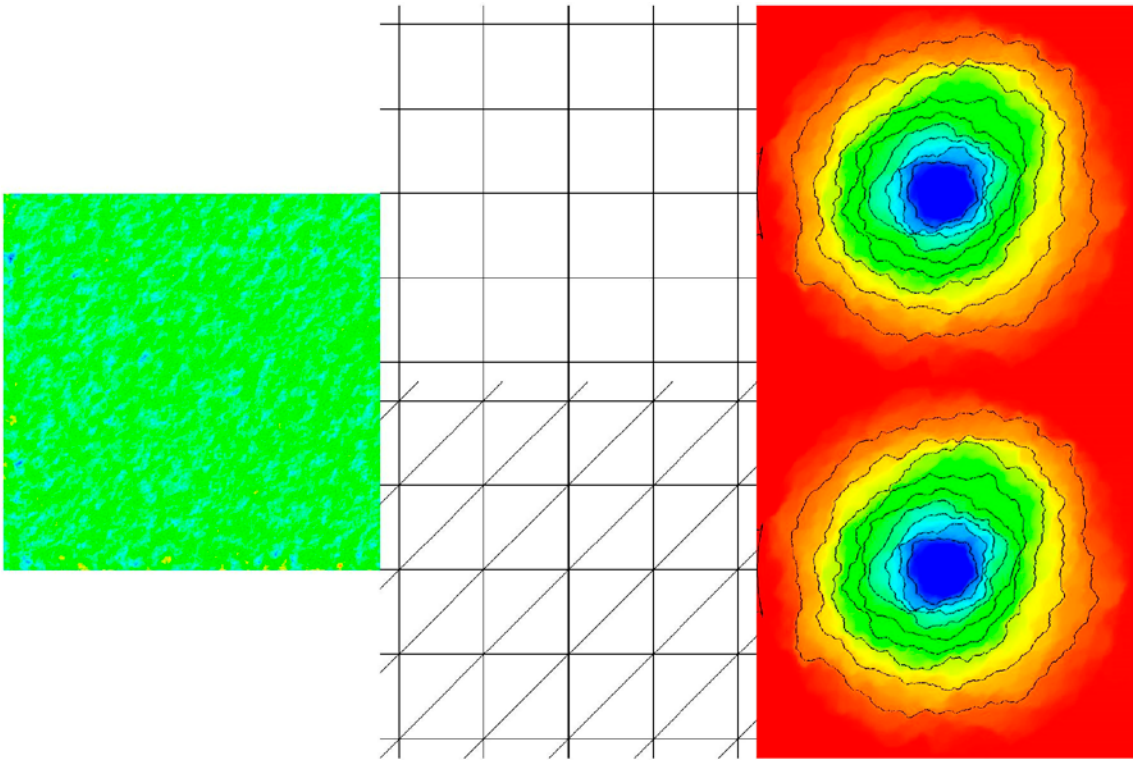

Figure 2-13. *The effect of the discretisation on the modelled domain. Left: the transmissivity field. Middle: two different finite element meshes. Right: hydraulic head.*

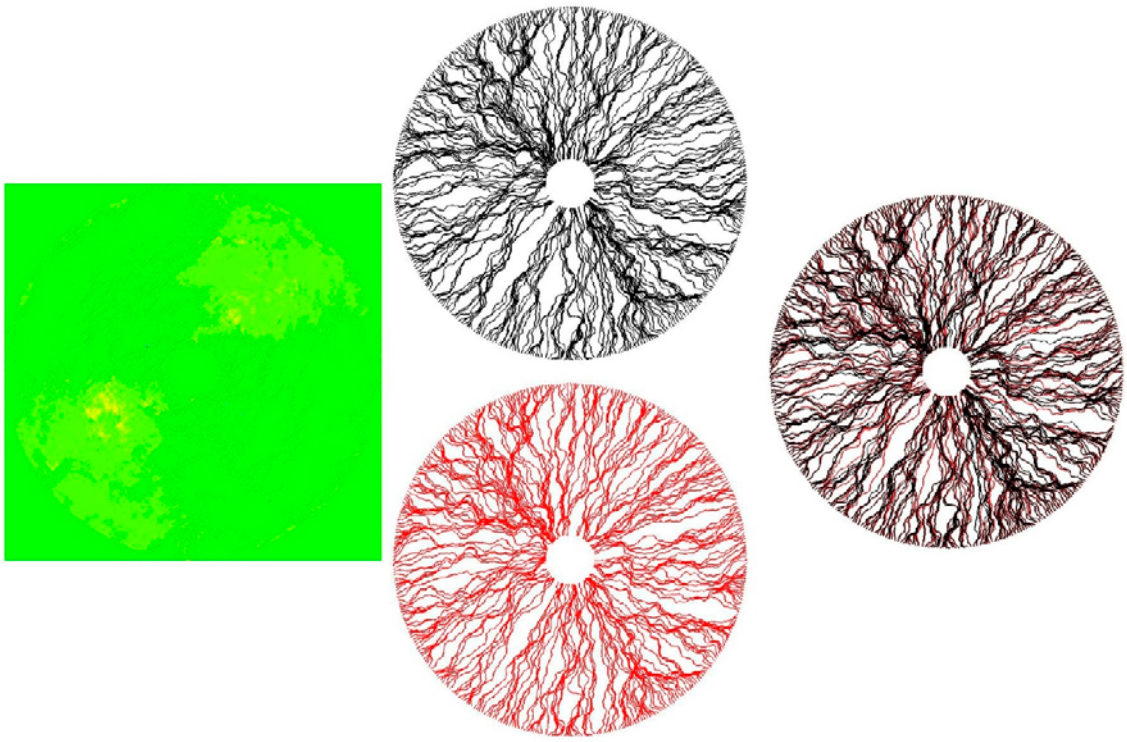

Figure 2-14. The effect of discretisation of the modelled domain (cont). Left: differences in the head fields obtained on the two different meshes. Middle: pathlines obtained from the two kinds of discretisation. Right: the superimposed sets of pathlines.

2.6.5 Revisiting TS28

In an attempt to unify approaches used in different scales, the block-scale TS28 simulation case of Task 7B was revisited so that the effect of a more elaborated microstructure in the large hydrogeological zones could be assessed. This effect was analysed in several settings of which four are documented here: using homogeneous zones and three spatially correlated Gaussian transmissivity fields as described above with varying correlation lengths (Figure 2-15).

All other input remained unchanged and the time-dependent head field was recalculated. The head along the pumped KR14 borehole and along five more observation holes was extracted from the final timestep of a single realisation (Table 2-4).

The largest difference between the final head fields using $l_T = 5$ m and $l_T = 20$ m as correlation lengths was over 12 m at the pumped borehole, whilst the difference in the observation holes remained much smaller, typically ~1–2 m.

Table 2-4. Variation of calculated head [m] in the open boreholes as the effect of the microstructure.

Borehole	Homogeneous zones, $T = T_{geom}$	Gaussian T, $l_T = 5$ m	Gaussian T, $l_T = 10$ m	Gaussian T, $l_T = 20$ m
KR14	−2.3	−1.2	−7.2	−13.7
KR15	4.3	4.6	4.7	2.8
KR16	4.9	4.9	5.1	3.5
KR17	5.1	5.1	5.3	3.7
KR18	4.4	4.6	4.6	2.6
KR30	5.1	4.5	4.9	3.7

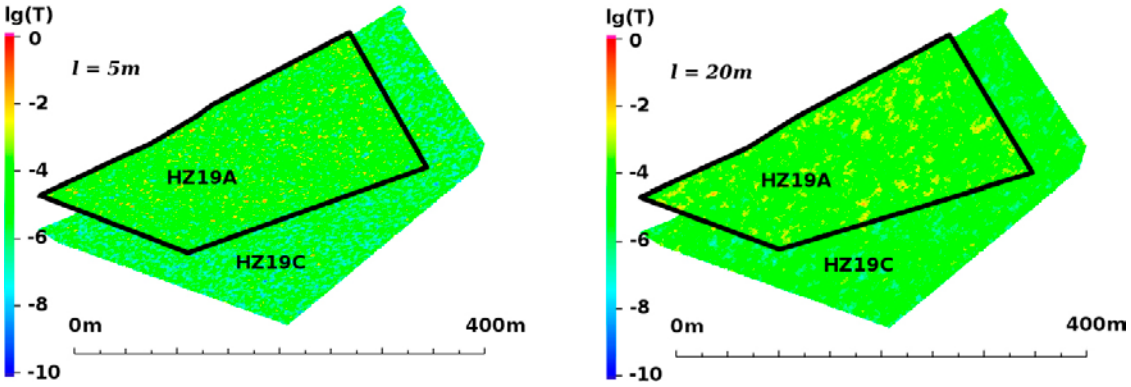

Figure 2-15. *Variation of transmissivity over HZ19A and HZ19C in cases with correlation lengths of l_T = 5 m and l_T = 20 m, respectively.*

2.7 Discussion and conclusions

2.7.1 Discussion of results

The results obtained from the numerical models described above *appear* to characterise the behaviour of the flow system *qualitatively correctly* in many respects. The distribution and variability of the calculated head field was in accordance with the expectations. The flow patterns that developed between the prescribed boundary conditions along the media of which properties were defined in several ways reflected both the geometry of the hydraulically active boundaries and the properties of the actual transmissivity distributions.

The uncertainties of these qualitatively apparently correct results may be attributed to the uncertainties of the basic assumptions, the input data and also to some numerical artefacts. The former can be determined by the assessment of the measurement error in the input. The latter may manifest itself in several forms and may be associated to almost any component of the numerical model and the tools that had created it.

Probably the most fundamental basic assumption was that the transmissivity field varies according to a spatially correlated Gaussian distribution, in other words we assume that the many factors participating in the genesis of the microstructure of the fracture all had a more or less equal contribution to it. In the lack of further data about the internal microstructure of the modelled fracture this assumption is appropriate – but not necessarily true. In case one or more factors played a more pronounced role in the formation of the fracture a non-Gaussian transmissivity distribution may have evolved. And even though the identification and the assessment of the weights of these factors are problematic and fell beyond the scope of this study, it is nonetheless conceivable that the transmissivity distribution is not Gaussian after all, even if no hard data would support this assumption.

Flow measurements in the nappy experiment were performed under physically difficult circumstances but with utmost care. It is believed that the applied method accurately determined the number of main exit points (peaks) of the flow from the fracture to the shaft and that the magnitude of these peaks are sufficiently close (within 10–20 %) to the reality. It has been documented that an unknown amount of grout powder covered part of the shaft wall, effecting the redistribution of the flow's exit points. Thus, independently of the uncertainties in the flow measurements other factors may have influenced the flow distribution along the shaft wall.

As for the boundary conditions, the values used as high head in the fracture and low head at the shaft could be measured with the highest accuracy of all input data, which was essential to operate with the right magnitude of the hydraulic gradient.

Spread of the transmissivities

The magnitude of the flows and the hydraulic gradient around the shaft are informative with respect to the mean transmissivity of the pierced fracture. However, flow characteristics and retention properties of the media also depend on the variability of the transmissivity around its mean. This spread is expressed as the standard deviation of the transmissivity distribution. It is essentially problematic to measure or even estimate this parameter, however, retention properties appear to be rather sensitive to it. Low spread means that the flow traverses areas of similar transmissivities before eventually reaching the low head boundaries at the shaft. In the case of high spread, chances are that the flow would encounter a particularly low transmissivity zone on its way to the shaft. Since there is no guarantee that the high transmissivity zones would get connected and thus offer a continuous pathway, travel times depend on the least transmissive zones along the pathlines. This effectively reduces the frequencies of pathlines characterised by low retention capabilities (Figure 2-10) whilst areas of high retention appear. Some parts of the fracture are never actually visited by the pathlines and act as dead or inactive zones even in the presence of extremely high hydraulic gradient and with some spots of high transmissivity in them, enclosed by areas of much lower transmissivity.

Because of the above, flow patterns that develop at higher spread of the transmissivity tend to exhibit fewer exit points at the shaft. The measured data show only a few such peaks, and this may be attributed to a relatively large spread in the transmissivities.

Note that often the spread of the observed transmissivities is too large to take into account in a numerical model.

Correlation length

Besides the mean and the spread, retention properties are also affected by the correlation length of the spatially correlated Gaussian transmissivity distribution. To assess this effect, with all other parameters left unchanged, the correlation length was varied in three steps: 0.27 m, 0.65 m and 1.09 m, which in the mesh extended over 5, 12 and 20 cells, respectively. The mechanism of this effect is related to the degree of channelization of the flow: the higher the correlation length, both low and high transmissivity zones extend farther and thus channels form more pronouncedly (Figure 2-7). The more channelized the flow is the poorer is the retention capability of the medium. When characterising the retention property with the *wl/q* quantity this phenomenon is readily seen in the *wl/q* frequency distribution (Figure 2-11).

As in the measured data there are only a few flow peaks at the shaft wall, this may suggest that the correlation length is over a metre assuming $\sigma(\lg(T)) = 1$ m^2/s as the spread of the transmissivity.

Non-symmetric low head BC

Besides the transmissivity distribution, the flow is also strongly affected by the boundary conditions. The flow measurements of the nappy experiment detected only a few peaks on a specific location of the shaft wall, which can be attributed both to the significantly channelized flow and/or the asymmetric boundary conditions prevailing there. It is actually known that some grout powder was sprayed into the southwestern wall of the shaft, however no data is available about its quantity.

To assess the role of this random grouting, the flow distribution at the shaft wall was recalculated in a sensitivity case where instead of the circular low head, no flow was assumed at the southwestern part (Figure 2-16). In this particular study the correlation length was 1.09 m (which extended over 20 elements in the mesh). The calculated pathlines reached the shaft, and passing by the wall section closed for the flow quit the fracture at the northeastern surface of the shaft wall. Similarly to the measured data, the distorted flow distribution exhibited only a few peaks remaining within 20% of the measured values (Figure 2-5), which may suggest that the observed flow distribution could also have been influenced by the conditions on the shaft wall.

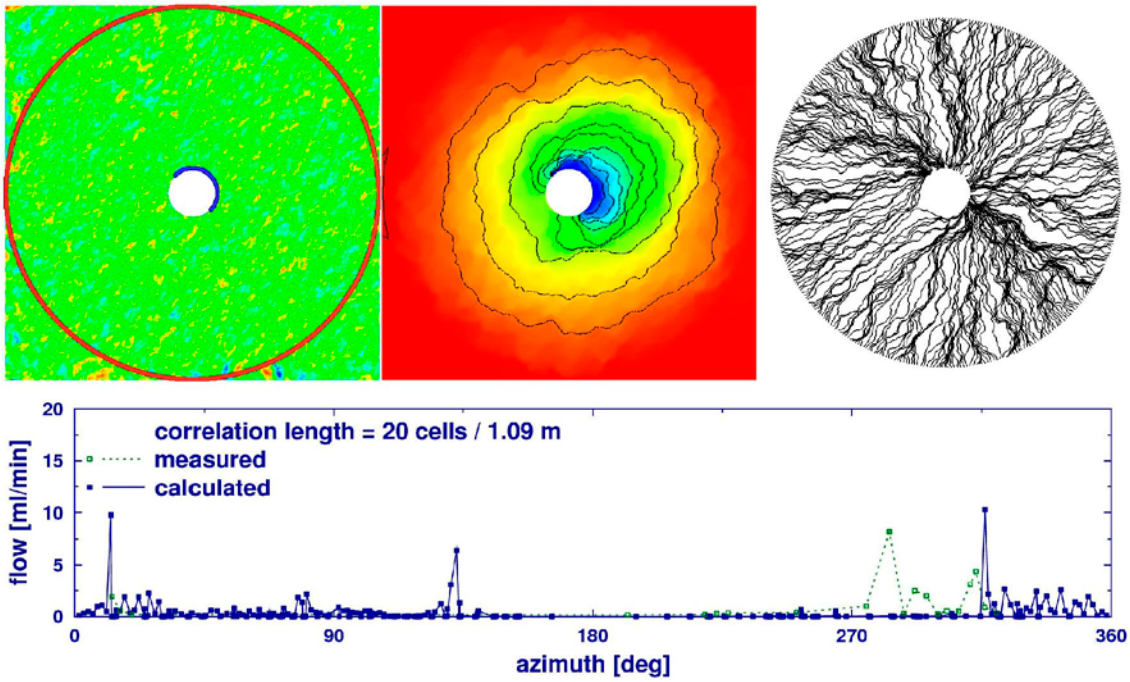

Figure 2-16. *The effect of non-symmetric low head boundary condition. Left: transmissivity field and the boundary conditions that define the flow. Middle: the distribution of hydraulic head. Right: flowpaths around the semi-closed shaft. Bottom: outflow distribution at the shaft wall – no outflow between 135 and 315 degrees.*

Model definition and scale

When determining the F-factor as a measure of retention, this result was calculated from all the available (usually twenty) realizations. However, in order to gain insight about the variability of this measure, in the case of one of the submodels (KU1_NS – in which the hydraulic gradient was set from south to north) hundreds of realizations were created and the variability of the F-factor was analysed for subsets of varying size in terms of frequency distributions. It was found that the frequencies of the log-F-factors, albeit clearly bounded, showed such a great variability that none of the subset frequencies appeared characteristic to the whole set representing the KU1 submodel. This might follow from a number of reasons, one of them being that if the dependence of the results on the realizations is greater than that on the model parametes, then the definition of the model on this scale may not be adequate, at least specifically for the F-factor calculations. As noted earlier, due to the two orders of magnitude smaller hydraulic gradient used in the F-factor calculations compared to that applied in the well tests (0.1 m/m and 12 m/m, respectively) the variability of the head field (which propagates to the pathlines and the retention properties) is much greater in the case of the former.

Terzaghi-correction

Having used data from the Simpevarp and Forsmark sites, Sweden, it has been shown (Davy et. al. 2006) that the Terzaghi-correction overestimates the fracture intensity necessarily leading to the overconnectedness of the model, and more elaborated correction schemes have been offered instead. However, in the case of mostly subhorizontal zones, like those occurring in the Task 7C models, this error is believed to be significantly smaller.

2.7.2 Numerical artefacts

The artefacts inevitably brought about by the numerical tools along the creation of the numerical model and the calculated results may be associated to the following circumstances (this list is not comprehensive).

Complexity of the media

The increase of the complexity of the flow system is primarily induced by the variability of the hydrogeological properties in it, and beyond a certain point numerical artefacts may develop in the results.

One of the common artefacts occurring in systems with a significant spread in their properties are the non-physical local minima or maxima in the results (e.g. head or concentration). These features, which do not follow from the boundary conditions, may compromise the calculation of the flow paths by a particle tracking algorithm and thus introduce further errors in the retention properties etc. (Note that this problem is independent from that of the discontinuous flow field usually characterizing results obtained from the finite element method, which also constitutes challenges to particle tracking algorithms.) With the increase in the spread of the transmissivity these artefacts manifest sooner or later, thus the monitoring of their appearance is appropriate. The head fields obtained in this study were checked for these local extrema and – most probably because of the large head gradient induced by the boundary conditions – no such artefacts were detected. Gradually increasing the variability in the transmissivity field caused poor or no convergence of the iterative calculations prior to non-physical extrema could develop. Theoretically, non-physical extrema of the calculated head field can be avoided by introducing corrective techniques along the solution (see e.g. Kuzmin and Turek 2002), however, this usually involves a major development effort.

Arithmetic precision

Particle tracking algorithms are known to be sensitive to the quality of the scalar field in which they are required to follow the trajectories. In this case the scalar field was that of the hydraulic head, which in some of the simulation cases was calculated with both single and double precision (REAL*4 and REAL*8 in Fortran notation). The particle tracking algorithm was implemented in a different piece of software, which read in the saved head field in the necessary precision. Also this software was attempted to run in single and double precisions, however, qualitatively correct or even meaningful results was only obtained from the version of the code run in double, with a few routines compiled even in quadruple (REAL*16) precision. Solely this fact underlines the significance of the employed arithmetic precision.

In addition, pathlines calculated from single-precision and double-precision head fields were compared with and without overlapping the two sets of trajectories. On the basis of this comparison the following can be observed (Figure 2-6):

- The pathlines significantly depend on the arithmetic precision used in calculating the head field.
- Pathlines obtained from double-precision heads appear to capture more details of the flow.
- Single-precision pathlines tend to show more channelized flow.

Thus it seems advisable to calculate the head field with the highest available precision when it comes to producing pathlines. Whether widening the representation of floating-point numbers beyond double-precision would further improve the results in terms of their eventual convergence at a certain precision is unclear.

Discretisation scheme

The base mesh, over which the transmissivity distribution is defined can be created with different types of finite elements. Customarily rectangular or triangular elements are used, with little or no considerations given to the appropriate element type. However, the finite element method facilitates the creation of two dimensional meshes using various elements (linear, quadratic or even higher order triangles or rectangles – Figure 2-13), even in the combination of different types. The choice of the element type depends on certain properties of the elements or to attain compatibility with the available visualizer, and it is usually taken for granted that – given a certain level of resolution – the chosen element type plays no significant role in defining the results.

This assumption was checked with simulations employing two different types of elements: linear rectangles and linear triangles at the same level of mesh resolution (Figure 2-13). The triangular elements were created by splitting the quadrats with their diagonals aligned. Note that the number and distribution of the Gaussian integration points within a base quadrat, and thus in the whole mesh, is different in the two cases (Figure 2-12).

With all other inputs unchanged, the head fields calculated over the two meshes show a comforting resemblance for the naked eye, however, the difference field already reveals the effect of the discretisation schemes (Figure 2-14). The distribution of the greatest head differences somewhat follows the alignment of the diagonals in the triangular mesh, whilst the magnitude of the head differences ranges from 0.0 to 0.6 m. Further, the pathlines obtained from the two head fields diverge to an even greater degree than the heads do. Having drawn the pathlines in two different colours for the two cases, in the case of identical results the superimposed image would only show the pathlines in one of the colours. However, the combined image reveals that the two sets of pathlines are far from matching each other.

Note that in this case the triangular elements *per se* cannot be considered inferior to the quadratic elements, even though the latter bear some favourable properties in the calculations. These properties cannot change the fact that the flow that follows from the imposed boundary conditions is largely radial, and thus crosses some of the quadrat elements along their diagonal, whilst others along their sides, effectively putting the numerical integration points in somewhat different roles in the course of the finite element analysis. Using a random alignment of triangular elements may handle this issue more efficiently.

Results, especially pathlines can vary from one finite element discretisation scheme to the other as much as they can vary between different realisations of the stochastic transmissivity field. This effect can be considered as a further numerical artefact in the results and should be eliminated by careful design and via the assessments of averaged variables obtained from several realisations.

2.7.3 Main conclusions

Task 7C was aiming at targets, about which a lot of good quality data became available and it was hoped that using these data the task would increase the understanding of the flow and transport processes on the canister scale. However, it was demonstrated that numerous factors could be influencing the calculated results, perhaps to the extent where their relevance can be challenged. Thus Task 7C transformed into an endeavour in which the understanding increased also in a different issue, namely the sensitivity of the calculated results with respect to some non-physical factors, like the algorithm generating the transmissivity field, the applied arithmetic precision, the quality of the calculated head field in terms of the non-physical local extrema or the discretisation scheme as well. Fortunately enough, these issues are not necessarily inherent in all the results and on the basis of these experiences similar issues may be avoided in the future.

It was observed by revisiting the TS28 simulation case that the influence of the microstructure in the fractures may have an effect also on the block scale. This finding is perhaps not intuitive at first, since the mean transmissivity, which defines the effective transmissivity of the hydrogeological zones remained unchanged.

2.7.4 Evaluation of conceptual models and modelling approach

The conceptual models developed in Task 7C1 constituted an appropriate basis for the numerical models built upon them, as the calculated results were – perhaps with the exception of the c-PP129-1 test – in very good agreement with the observations with no or minimal prior calibration. The role of the stochastic components of the models is probably not very significant as in this setup the background fractures did not add to the effective transmissivity of the system too much.

The only necessary new element in the modelling approach was the step of producing the microstructure of the fracture, which was defined as a spatially correlated Gaussian T-field conditioned on the observations. This move proved inevitable as without a microstructure in the fracture the observed flow distribution of Task 7C3 could not be reproduced. The significance of model conditioning appeared beneficial, although no test was initiated to assess a non-conditioned model.

The numerical implementation of the matrix factorization algorithm responsible for the generation of the transmissivity field was rather challenging, primarily because no direct verification of the correctness of the generated field was readily available.

References

SKB's (Svensk Kärnbränslehantering AB) publications can be found at www.skb.com/publications.

Chen Y, Zhang D, 2006. Data assimilation for transient flow in geologic formations via ensemble Kalman filter. Advances in Water Resources 29, 1107–1122.

Davy P, Darcel C, Bour O, Munier R, de Dreuzy J R, 2006. A note on the angular correction applied to fracture intensity profiles along drill core. Journal of Geophysical Research 111, B11408. doi:10.1029/2005JB004121

Dietrich C R, Newsam G N, 1996. A fast and exact method for multidimensional Gaussian stochastic simulations: extension to realizations conditioned on direct and indirect measurements. Water Resources Research 32, 1643–1652.

Evensen G, 2009. Data assimilation: The Ensemble Kalman Filter. 2nd ed. Berlin: Springer.

Felicismo A, Cuetos J C R, Garcia M E P, Cuartero A, Rodriguez P G, 2011. VecStatGraph3D. Vector analysis using graphical and analytical methods in 3D, R package. Available at: https://gim.unex.es/VecStatGraphs3D/

Keto V, Koskinen L, 2009. Äspö Hard Rock Laboratory. Äspö Task Force on modelling groundwater flow and transport of solutes – Task 7A: Subtask 7A1. SKB ITD-09-06, Svensk Kärnbränslehantering AB.

Konikow L F, Hornberger G Z, 2006. Modeling effects of multinode wells on solute transport. Groundwater 44, 648–660.

Kuzmin D, Turek S, 2002. Flux correction tools in finite elements. Journal of Computational Physics 175, 525–558.

Lund U, Agostinelli C, 2010. Circular statistics. R port of the S-plus CircStats package. Available at: http://cran.r-project.org/web/packages/CircStats/

Löfman J, Mészáros F, 2013. FEFTRA™. Verification – Update 2013. Posiva Working Report 2013-60, Posiva Oy, Finland.

Matsumoto M, Nishimura T, 1999. A C-program for MT19937. Available at: http://www.math.sci.hiroshima-u.ac.jp/~m-mat/MT/VERSIONS/FORTRAN/TAKANO/mt19937.f

Pekkanen J, 2009a. Difference flow measurements in ONKALO at Olkiluoto, drillholes ONK-PP122–ONK-PP124, ONK-PP126, ONK-PP128, ONK-PP131, ONK-PP134 and ONK-PP137. Posiva Working Report 2009-04, Posiva Oy, Finland.

Pekkanen J, 2009b. Difference flow measurements and hydraulic interference test in ONKALO at Olkiluoto, drillholes ONK-PP125, ONK-PP127 and ONK-PP129. Posiva Working Report 2009-40, Posiva Oy, Finland.

Ruan F, McLaughlin D, 1998. An efficient multivariate random field generator using the fast Fourier transform. Advances in Water Resources 21, 385–399.

Vidstrand P, Ahokas H, Bockgård N, Dershowitz W, Holton D, Lanyon W, Poteri A, Koskinen L, 2015. SKB Task Force GWFTS – Task 7 Descriptions for hydrogeological modelling of Olkiluoto, Finland. Compilation of all task descriptions assessed within the Task 7 of the SKB Task Force on modelling of groundwater flow and transport of solutes. SKB P-12-21, Svensk Kärnbränslehantering AB.